Journal of Nanobiotechnology

RESEARCH

Open Access

# Enhanced therapeutic effects of all-trans retinoic acid nanostructured lipid carrier composite gel drug delivery system for alopecia areata

Lingling Zheng[1,2], Yang Du[1], Lulu Zhang[1,3], Fuxing Jin[1,3], Wangting Li[1], Xuan Zhou[1], Yanping Yin[1,4], Yan Weng[1*], Dong Xu[1*] and Jingwen Wang[1*]

## Abstract

**Background** Alopecia areata (AA) affects approximately 2% of the global population and causes psychological distress. All-trans retinoic acid (ATRA) has the potential to promote hair regeneration; however, its clinical use is limited by skin irritation and low targeting specificity. To address these limitations, we designed an ATRA-loaded nanostructured lipid carrier gel (ATRA-NLC-Gel) drug delivery system to enhance the therapeutic effects of ATRA in AA.

**Results** ATRA-NLC showed a uniform nanoparticle size distribution and excellent biocompatibility. In vitro, they enhanced the uptake ability of dermal papilla cells, increased cell viability, and promoted cell proliferation by facilitating the cell cycle process. Compared to ATRA cream, ATRA-NLC-Gel significantly reduced skin irritation, prolonged residence time on the skin, and achieved a sustained and slow release of ATRA. Treatment with ATRA-NLC-Gel enhanced transdermal penetration and targeted enrichment in the hair follicle region, thereby significantly promoting hair regrowth. ATRA-NLC-Gel improved AA symptoms by upregulating CD200 and Ki-67 expression, activating the Wnt/β-catenin pathway.

**Conclusions** ATRA-NLC-Gel enhanced the transdermal permeability and follicle-targeting efficacy of ATRA, alleviated ATRA-induced skin dryness and irritation, and effectively improved the symptoms of AA in AA model mice. ATRA-NLC-Gel offers a highly promising strategy for transdermal treatment of AA in clinical setting.

## Highlights

ATRA-NLC-Gel effectively prevented skin irritation by a slow and controlled release behavior of ATRA.

ATRA-NLC-Gel exhibited more pronounced transdermal permeability and follicular targeting properties.

*Correspondence:
Yan Weng
guowawa521@163.com
Dong Xu
dongxu418@163.com
Jingwen Wang
wangjingwen8021@163.com

Full list of author information is available at the end of the article

ATRA-NLC-Gel significantly restored the follicular immune homeostasis, promoted hair follicle cell proliferation, and enhanced hair regrowth in AA model mice.

**Keywords** Nanostructured lipid carrier, All-trans retinoic acid, Alopecia areata, Drug delivery system, Hair regeneration

**Graphical Abstract**

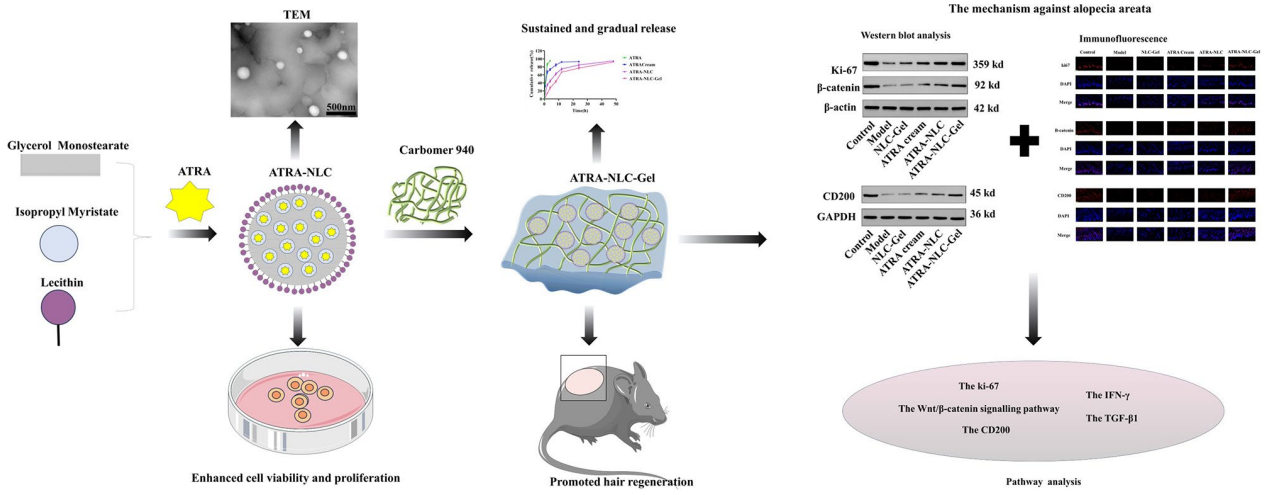


## Introduction

Alopecia areata (AA), a common autoimmune disorder in clinical practice, affects approximately 2% of the global population, spanning young and middle-aged individuals without sex or geographical boundaries [1]. Moreover, patients with AA face a higher risk of developing other autoimmune diseases compared to the general population [2–4], which undoubtedly complicates disease and imposes a heavy psychological burden on patients. It is widely accepted that loss of hair follicle immune privilege is a key factor in the pathogenesis of AA [5]. Furthermore, genetic predisposition [6] and environmental factors [7, 8] are also regarded as exerting certain influences on the initiation and advancement of this disease. These factors interact and collectively contribute to the occurrence and progression of AA, causing significant psychological and physiological stress to patients. Clinical studies have disclosed that apart from the characteristic patchy hair loss as the main manifestation, there is a remarkable high expression of IFN-γ in the area of the skin lesion [9, 10]. Meanwhile, the expression levels of immune regulatory molecules CD200 [11] and TGF-β1 [12] at the hair follicle site have been decreased significantly. It is worth noting that both the proliferation marker Ki-67 of hair follicles [13] and β-catenin [14], which influences the activation of hair follicle stem cells, show abnormally low expression as well. Current clinical treatment strategies for AA include topical application of glucocorticoids, minoxidil, and other medications [15, 16], oral JAK inhibitors [17], hair transplantation surgery [18], and microneedle-mediated therapy [19]. However, these treatment methods exhibit varying degrees of limitations. Topical medications may induce allergic reactions, while pain associated with microneedle therapy reduces patient adherence to treatment. Oral medications and hair transplantation surgeries can be expensive for some patients.

All-trans retinoic acid (ATRA), an active metabolite of vitamin A in vivo, plays a pivotal role in regulating epithelial cell differentiation, proliferation, and immune responses [20–22]. Studies have revealed that the topical application of ATRA at a concentration of 0.025% effectively promotes hair growth [23]. Wen et al. have reported that ATRA acts on hair follicle stem cells in androgenic alopecia by upregulating CD200 protein expression and activating the Wnt/β-catenin signaling pathway, thereby regulating hair growth [24]. Notably, studies have demonstrated that ATRA is capable of modulating the lineage plasticity of hair follicle stem cells to facilitate hair regeneration [25], and also inhibits the production of IFN-γ through the regulation of immune cell functions [26]. These reports collectively indicate that ATRA holds great potential for the treatment of AA. Nevertheless, ATRA has limited clinical application because of its inferior stability, poor water solubility(< 1 mg/mL) [27], and high lipophilicity (log $P \approx 6.3$) [28], and commercial ATRA creams present poor skin permeability and skin irritation [29]. Consequently, the development of novel ATRA formulations for the treatment of AA emerges as a critical priority.

Nanostructured lipid carriers (NLC) refer to a category of delivery systems with a particle size ranging from 10 to 1000 nm [30]. The minuscule particle size of NLC allows them to be in close contact with the stratum corneum and form an effective occlusive barrier on the skin surface, which enhances skin hydration and consequently expands the intercellular spaces within the stratum corneum [31–34]. This creates pathways for drug molecules to penetrate into deeper layers, thereby significantly improving the transdermal permeation efficiency of bioactive compounds [35, 36]. Moreover, encapsulating the active ingredient within NLC enables controlled drug release and enhances stability. Particularly notable is that related study has successfully observed nanoscale lipid carriers of approximately 300 nm in the interfollicular regions of the skin [37]. Yin-Ku Lin et al. developed diphencyprone-loaded NLC to enhance transdermal drug absorption and follicle-targeted treatment of AA [38]. The NLC loaded with tofacitinib were formulated to improve transdermal absorption and follicle-targeting efficacy for the treatment of AA [39]. Additionally, a complex of minoxidil and latanoprost was formulated into NLC for targeted local treatment of hair loss [40]. Collectively, these studies have demonstrated the substantial potential of NLC in skin penetration and follicle-targeted delivery. However, the high mobility of NLC may impede the retention of drugs on the skin surface [41].

Here, we aimed to encapsulate ATRA into NLC (Fig. 1), which can closely adhere to the skin, forming an effective occlusive barrier that enhances skin hydration, thereby facilitating the interaction between the drug and the stratum corneum, promoting the transdermal permeation of ATRA, and enabling its targeted enrichment in the hair follicles. Moreover, ATRA-NLC are dispersed into

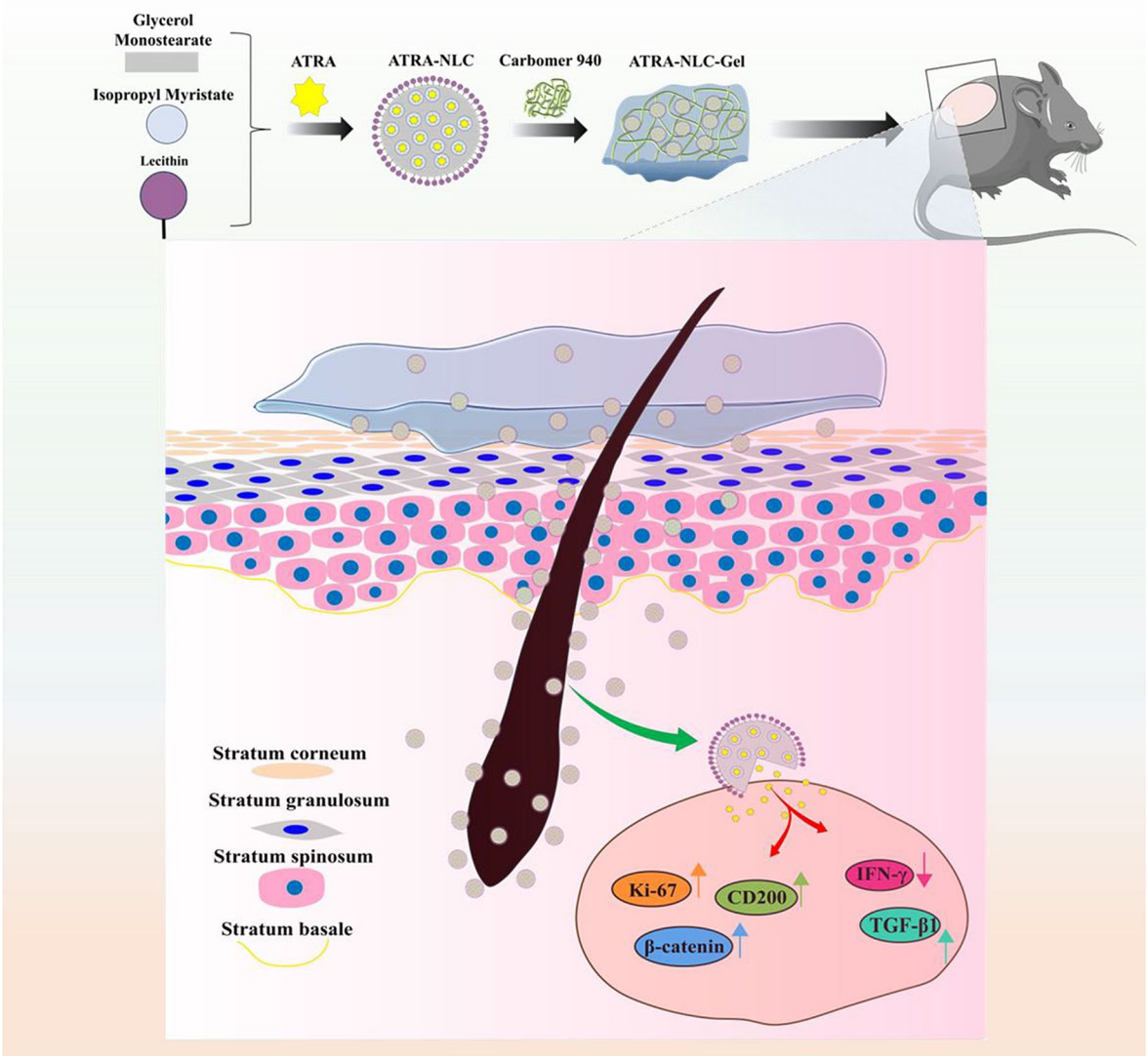


**Fig. 1** A schematic illustration of ATRA-NLC-Gel preparation and its promoting effect on hair regeneration

a gel matrix to construct the ATRA-NLC-Gel composite drug delivery system. This system not only protects ATRA-NLC from external environmental influences but also leverages the adhesive and sustained-release properties of the gel to form a local drug reservoir on the skin surface, achieving continuous drug release, significantly enhancing transdermal absorption efficiency and enriching ATRA in the hair follicles. Therefore, ATRA-NLC-Gel prolongs the drug's residence time in the skin and reduces the frequency of administration, thereby enhancing the therapeutic efficacy in AA mouse models.

## Results and discussion

### Characterization of ATRA-NLC

As shown in Fig. 2A, the ATRA-NLC is milky-white homogeneous opaque dispersion liquid. The image of transmission electron microscopy (TEM) (Fig. 2B) revealed that ATRA-NLC had an approximately spherical appearance, with uniform particle size and no adhesion. Compared to ATRA-NLC, Blank-NLC showed no significant difference in morphology (Fig. S1 A). The particle size of ATRA-NLC was approximately 180.2 ± 7.2 nm (Fig. 2C). According to previous studies [42–45], nanoparticles within this size range are more inclined to target and deliver encapsulated drugs to hair follicles, which is also the objective of this study. The particle size of Blank-NLC was 176.4 ± 8.3 nm (Fig. S1 B), showing minimal change compared to ATRA-NLC. This suggests that the interaction force between ATRA and the carrier is weak, and its incorporation does not significantly alter the particle size of the carrier. This stability may result from the solid/liquid lipid mixed framework structure of the nanostructured lipid carrier, which enables high drug-loading capacity and stability. When encapsulated

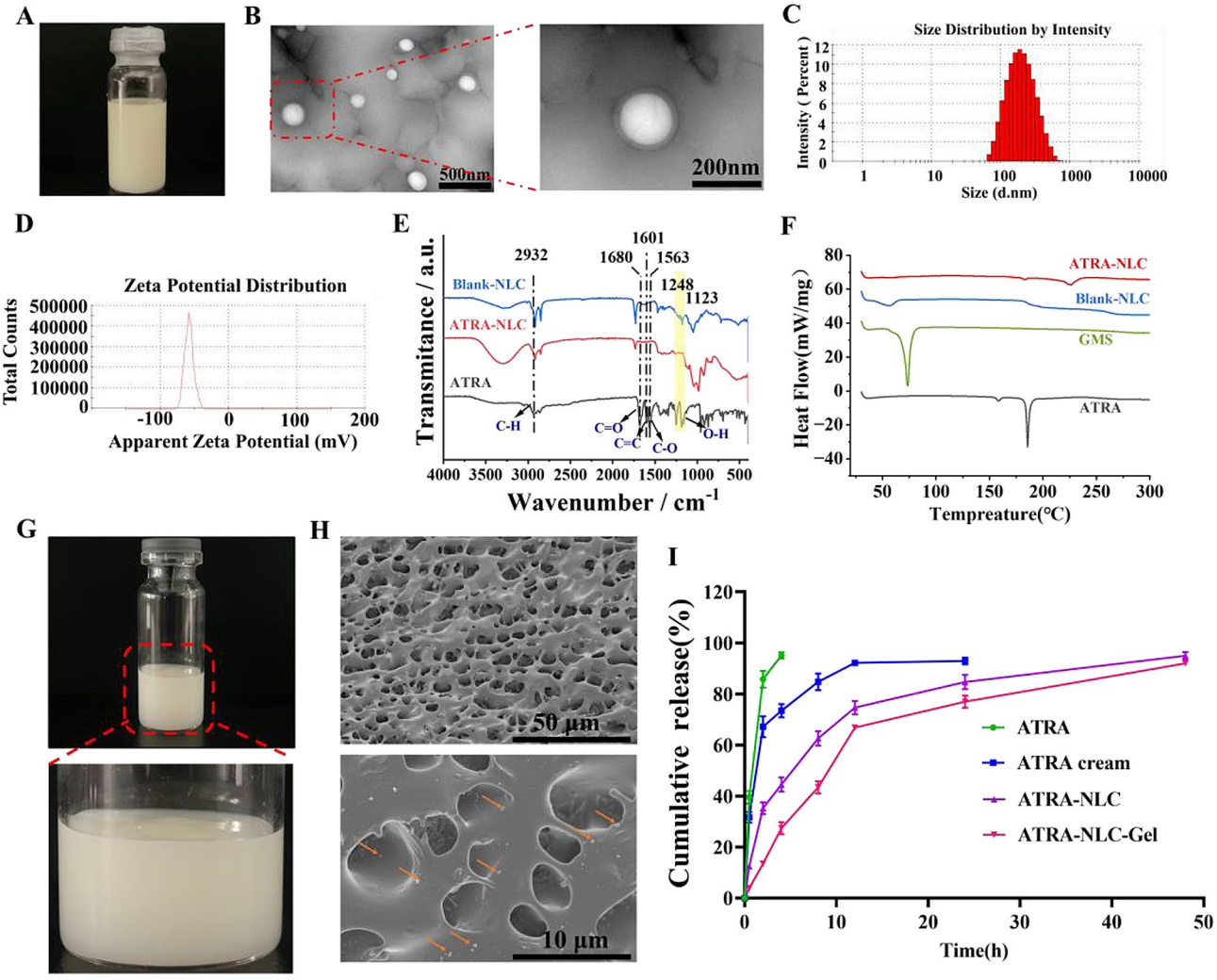


**Fig. 2** Characterization of ATRA-NLC and ATRA-NLC-Gel. **(A)** Appearance of ATRA-NLC. **(B)** TEM images of ATRA-NLC. Scale bar: 200 nm and 500 nm. **(C, D)** Particle size distribution and zeta potential of ATRA-NLC. **(E)** FT-IR spectra for Blank-NLC, ATRA-NLC, ATRA. **(F)** Differential scanning calorimetric (DSC) thermogram. **(G)** Appearance of ATRA-NLC-Gel. **(H)** SEM image of the ATRA-NLC-Gel. The yellow arrow points to ATRA-NLC. Scale bar: 50 μm and 10 μm. **(I)** Release behavior of different formulations of ATRA

within the carrier, drug molecules uniformly fill the irregular lattice structure of the lipid framework. The polydispersity index (PDI) values were employed to characterize the size distribution of the nanoparticles. The results demonstrated that the PDI of both ATRA-NLC and Blank-NLC was less than 0.2, indicating a narrow size distribution and uniform particle size [46]. Zeta potential, a crucial parameter for nanosolutions, reflects the surface charge characteristics and stability of the nanoparticles [47]. The zeta potential of ATRA-NLC was − 57.8 ± 3.1 mV (Fig. 2D), indicating relatively high system stability. The drug-loading efficiency of ATRA-NLC was (7.4 ± 0.9)%, and the encapsulation efficiency was (95.7 ± 1.6)%. The Fourier Transform Infrared Spectroscopy (FT-IR) analysis provided a clear representation of significant changes in the characteristic spectral peaks of ATRA within the ATRA-NLC. Specifically, ATRA's signature vibrational modes, including the C-H stretching vibration peak of the $CH_3$ group at 2932 $cm^{-1}$, the C = O carbonyl stretching vibration peak at 1680 $cm^{-1}$, and the C = C and C-O stretching vibration bands at 1601 $cm^{-1}$ and 1563 $cm^{-1}$, and the O-H stretching vibration bands at 1248 $cm^{-1}$ and 1123 $cm^{-1}$, underwent shifts or complete disappearance (Fig. 2E). Further observations revealed that the infrared spectra of Blank-NLC and ATRA-NLC almost completely overlapped, with no new characteristic peaks observed. This phenomenon not only robustly demonstrates the absence of chemical interactions between ATRA and pharmaceutical excipients, but also unequivocally indicates successful and effective incorporation of ATRA into NLC [48]. The physical states of ATRA-NLC, Blank-NLC, glyceryl monostearate (GMS), and ATRA were investigated by differential scanning calorimetry (DSC). The results indicated that no distinct melting peaks were observed in the DSC thermograms of both Blank-NLC and ATRA-NLC. Compared with GMS, the melting peaks of GMS were not observed in both Blank-NLC and ATRA-NLC. This might be attributed to the addition of the liquid lipid isopropyl myristate, which disrupted the original lattice structure of the solid lipid GMS, thereby promoting the formation of a more disordered and imperfect crystalline structure, resulting in the disappearance or alteration of the melting peaks. Notably, the DSC thermogram of ATRA-NLC did not exhibit the characteristic melting peak of ATRA, strongly suggesting that ATRA has been effectively encapsulated into NLC [49] (Fig. 2F).

**Table 1** Fitting analysis of ATRA in different formulations

| Formulations | Model | Regression equation | $R^2$ |
|---|---|---|---|
| ATRA | Zero-order | $Q = 22t + 19.28$ | 0.7135 |
| | First-order | $Q = 96.8367(1\text{-}e^{-1.06t})$, | 0.9998 |
| | Higuchi | $Q = 49.88t^{1/2} + 3.7$ | 0.3727 |
| ATRA cream | Zero-order | $Q = 2.9t + 42.35$ | 0.4023 |
| | First-order | $Q = 87.8806(1\text{-}e^{-0.71t})$ | 0.9722 |
| | Higuchi | $Q = 18.32t^{1/2} + 23.10$ | 0.7382 |
| ATRA-NLC | Zero-order | $Q = 1.7t + 30.34$ | 0.6102 |
| | First-order | $Q = 88.9106(1\text{-}e^{-0.18t})$ | 0.9737 |
| | Higuchi | $Q = 14.15t^{1/2} + 11.83$ | 0.8854 |
| ATRA-NLC-Gel | Zero-order | $Q = 1.9\,t + 17.35$ | 0.7450 |
| | First-order | $Q = 91.9462(1\text{-}e^{-0.09t})$ | 0.9899 |
| | Higuchi | $Q = 14.86t^{1/2} - 0.8163$ | 0.9353 |

### Characterization of ATRA-NLC-Gel

The ATRA-NLC-Gel exhibited a pale yellow semisolid appearance. (Fig. 2G). Scanning electron microscopy (SEM) revealed a uniform and highly ordered three-dimensional porous structure within the gel, with ATRA-NLC particles evenly distributed as spherical shapes throughout the gel network (Fig. 2H). Numerous studies have revealed that this type of three-dimensional grid configuration effectively enhances the dispersion of nano-liquids, prevents the aggregation of nanoparticles caused by interparticle interactions, and significantly improves the overall stability of the composite gel system [50–52]. Furthermore, our research revealed an intriguing phenomenon compared to the Blank-Gel (Fig. S2), ATRA-NLC-Gel exhibited a more compact gel void structure. This finding can be ascribed to the remarkable interactions that occurred between ATRA-NLC and the internal crosslinking network of the gel during the drug-loading process. These interactions enhanced the crosslinking density, causing the gel wall structure to become more continuous and denser, eventually leading to pore shrinkage [53].

The preparation of the ATRA-NLC-Gel was intended to optimize the sustained-release of ATRA from the skin. As shown in Table 1, the drug release of ATRA, ATRA cream, ATRA-NLC, and ATRA-NLC-Gel conformed to the characteristics of a first-order pharmacokinetic model. The release rate of free ATRA was the fastest(Fig. 2I), and the cumulative release rate reached approximately 85.8% within 2 h and was almost completely released within 4 h. This phenomenon may be attributed to the fact that free ATRA is directly exposed to the release medium, thereby facilitating its rapid dissolution and diffusion. Such rapid release may lead to a swift increase in drug concentration at the site of administration, which in turn could potentially induce skin irritation [54]. The cumulative release rate of the ATRA cream at 2 h was approximately 67.1%, but it was nearly completely released within 24 h, with a cumulative release rate of approximately 92.9%. In contrast, the release rates of ATRA-NLC and ATRA-NLC-Gel were significantly slower, demonstrating their excellent sustained-release properties. At 24 h, the cumulative release rate of ATRA-NLC was approximately 84.6%, and that of ATRA-NLC-Gel was slightly lower at approximately

76.9%. This slower release could be attributed to the need for ATRA-NLC in the ATRA-NLC-Gel to first be released from the three-dimensional reticular structure of the gel, thereby delaying drug release. This characteristic contributes to the formation of a reservoir effect of the drug on the skin, enabling continuous and slow release, prolonging the drug's action time and reducing both the frequency of administration and potential skin irritation. By 48 h, the cumulative release rates of ATRA-NLC and ATRA-NLC-Gel were 94.9% and 92% respectively. Overall, by comparing the release characteristics of different ATRA preparations, we discovered that ATRA could achieve a sustained and slow drug release behavior when fabricated into ATRA-NLC and ATRA-NLC-Gel, effectively regulating the release rate of ATRA and facilitating to enhance its therapeutic effects on AA.

### Stability of ATRA-NLC-Gel

The stability experiments were carried out in accordance with International Council for Harmonization (ICH) Guideline Q1A(R2) (2003) [55]. Over five months, the appearance of the ATRA-NLC-Gel showed no significant changes and maintained a uniform texture (Fig. 3A). The particle size and PDI values increased slightly over

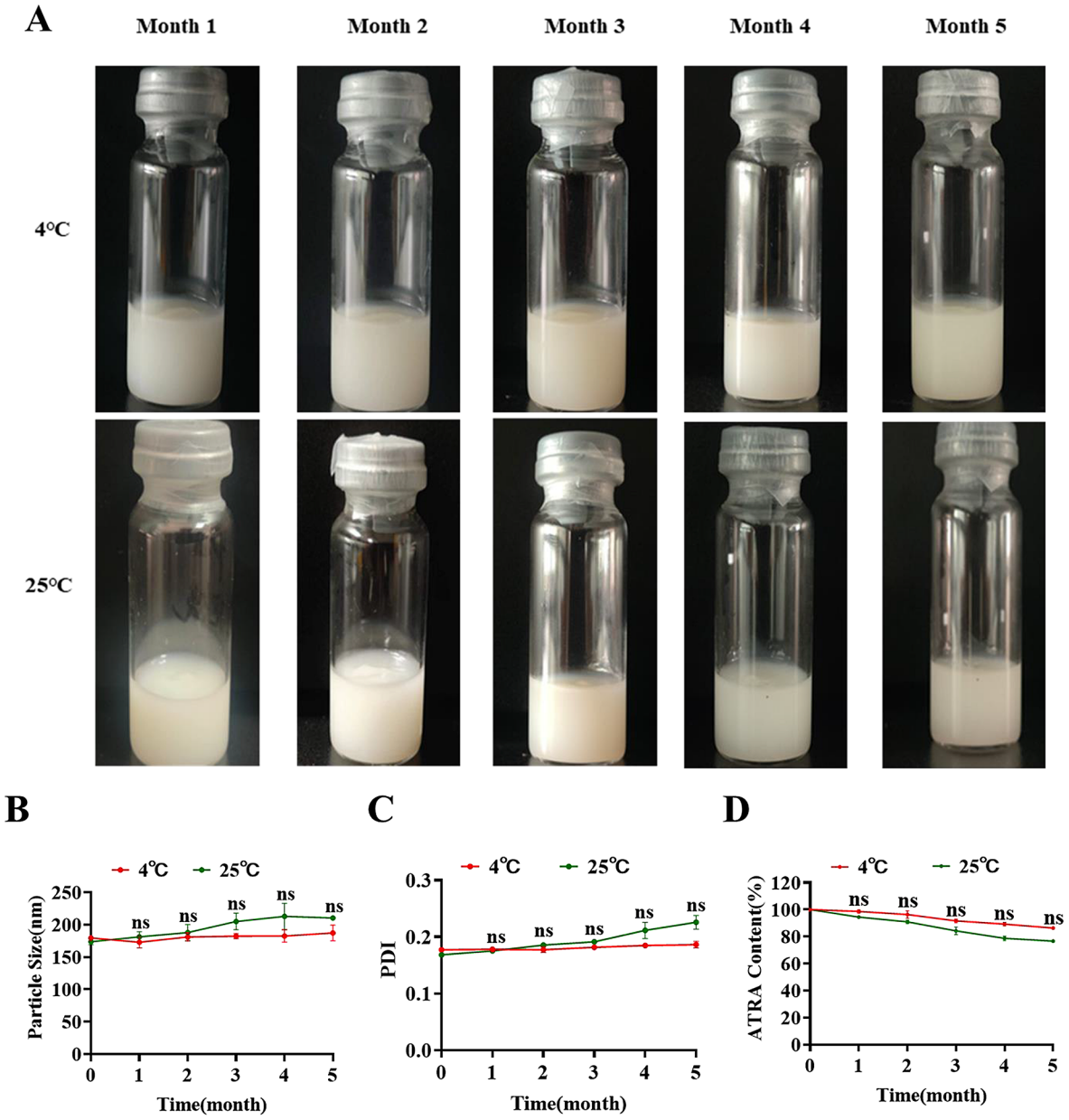


**Fig. 3** Stability of ATRA-NLC-Gel over 5 months under storage conditions of 4 °C and 25 °C. **(A)** Changes in the appearance of ATRA-NLC-Gel. Particle size **(B)** and PDI **(C)** variations of ATRA-NLC within ATRA-NLC-Gel. **(D)** Changes in ATRA content within ATRA-NLC-Gel $n = 3$, ns: no significant

time, accompanied by a minor decrease in the drug content (Fig. 3B&C). Under both 4 °C and 25 °C conditions, the particle size remained below 220 nm, the PDI stayed under 0.3, and the drug content percentage exceeded 70% (Fig. 3D). Statistical analysis showed no significant changes in particle size, PDI, and ATRA content over five months. Taken together, these results suggest that ATRA-NLC-Gel remained a good stability at 4 °C and 25 °C.

#### Safety evaluation of ATRA-NLC-Gel in vitro and in vivo

DPCs are crucial for hair follicle morphogenesis, growth cycle regulation, and maintenance of hair growth and development [56]. Therefore, DPCs were selected as the in vitro cell model to assess the impact of ATRA-NLC-Gel on cell viability and in vitro safety using the CCK-8 assay. Within the drug concentration range of 0.2–1 μg/mL, DPCs were incubated with ATRA cream, ATRA-NLC and ATRA-NLC-Gel for 24 h respectively. The results showed that the cell viability in the ATRA cream-treated group was approximately 90 – 100%, while the ATRA-NLC and ATRA-NLC-Gel-treated groups exceeded 100% (Fig. 4A). These findings indicate that, compared with ATRA cream, ATRA-NLC and ATRA-NLC-Gel exhibit no cytotoxicity and better biocompatibility, along with superior proliferative potential. Particularly, at a drug concentration was 0.6 μg/mL, the cell viability reached its peak, making this the optimal concentration for subsequent cell experiments.

The multiple skin irritation test is a methodology for evaluating the potential skin irritation caused by pharmaceuticals. Healthy SD rats underwent multiple skin irritation tests on their dorsal skin. The experimental results indicated that ATRA-NLC-Gel effectively reduced the local irritation associated with ATRA administration. Over the 14-day experimental period, neither the saline group nor the ATRA-NLC-Gel group exhibited erythema or edema at the administration site (Fig. 4B). This effect may be ascribed to the moisturizing property of ATRA-NLC-Gel, which help prevent epidermal water loss, enhance skin moisture and hydration, and mitigate irritation induced by direct exposure to ATRA. This observation aligns with prior reports on the excellent biosafety of flurbiprofen-loaded NLC-Gel, confirming their advantages in reducing skin irritation and improving skin tolerance [57]. In the free ATRA group, distinct erythema and mild edema appeared from Day 3 to Day 9 at the drug application site. This irritation gradually subsided from Day 12 to Day 14, likely due to the skin developing tolerance to retinoic acid [58]. On Day 9, the irritation score reached a peak, specifically 2 ± 0.8 (Fig. 4C), indicating mild irritant skin damage associated with this route [59]. Similarly, a commercially available ATRA cream demonstrated mild skin irritancy. This may be attributed to the poor skin permeability of ATRA cream, which leads to a rapid increase in the local concentration of ATRA on the skin surface following topical administration, thereby exerting a certain degree of irritancy on the skin [54].

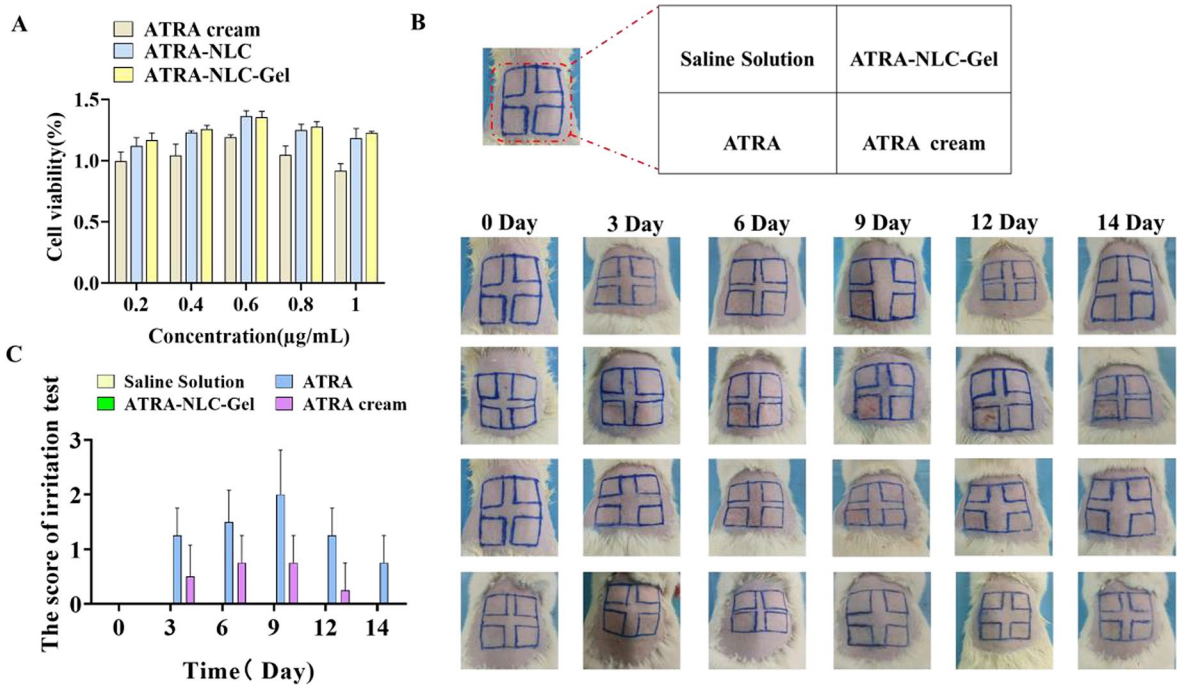


**Fig. 4** The safety evaluation of ATRA-NLC-Gel in vitro and in vivo. **(A)** Cytotoxicity of ATRA cream, ATRA-NLC and ATRA-NLC-Gel on DPCs, $n = 6$. **(B)** Images of SD rats' dorsal skin irritation after administration. **(C)** The skin irritation scores of each group, $n = 4$

Overall, these comprehensive in vivo and in vitro evaluations demonstrated that the ATRA-NLC-Gel possesses excellent biocompatibility, making it safe and non-irritating for topical application.

### Cellular uptake

Coumarin 6 (COUR 6) is a hydrophobic fluorescent dye. Owing to its outstanding fluorescence characteristics and low toxicity, it is frequently employed to label nanoparticles for simulating the active ingredients in drug delivery systems, facilitating the visualization analysis of cellular uptake and drug distribution [60, 61]. Hence, the effects of different formulations on DPCs uptake were compared using COUR 6 as the fluorescent probe. Based on the results of confocal laser scanning microscopy (CLSM; Nikon, Japan) (Fig. 5A), the fluorescence intensities in the COUR 6-NLC group were significantly higher than those in the free COUR 6 and COUR 6-Cream groups at all time points, suggesting that the COUR 6-NLC formulation was more effective in promoting the cellular absorption of COUR 6. Consistent with the CLSM observations, flow cytometry-based fluorescence quantification also

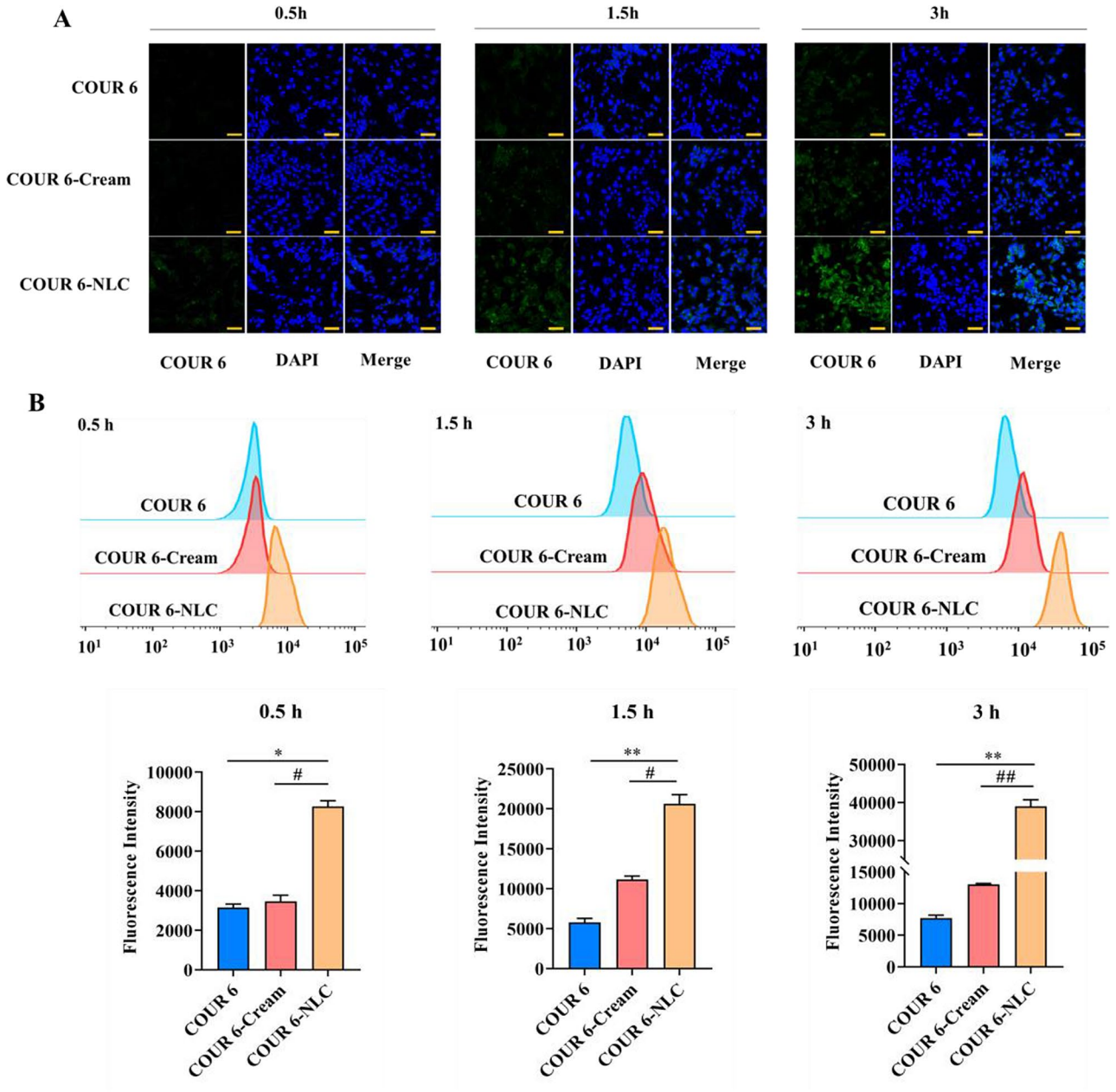


**Fig. 5** Cellular uptake of COUR 6-labeled preparations. **(A)** Cellular uptake assayed by CLSM. Scale bar: 50 μm. **(B)** Cellular uptake quantitatively assayed by flow cytometer (FCM). $n = 3$, $^{*}p < 0.05$, $^{**}p < 0.01$, vs. COUR 6; $^{\#}p < 0.05$, $^{\#\#}p < 0.01$, vs. COUR 6-Cream

confirmed that COUR 6-NLC significantly enhanced uptake by DPCs ($p < 0.01$) in a time-dependent manner (Fig. 5B). This phenomenon may be related to the nanoscale size effect and excellent biocompatibility of the NLC. The small size of the carrier facilitates easier access to and penetration through the cell membrane, whereas auxiliary ingredients such as lecithin possess excellent biocompatibility, thereby enhancing cellular uptake [62].

### In vivo skin permeation and distribution

Upon local dermal application, various COUR 6-labeled formulations exhibited skin penetration and retention tendencies similar to the cell uptake outcomes. At 0.5 h after local application, all formulations uniformly covered the skin surface as evidenced by the fluorescence intensity observed across the skin (Fig. 6A). This indicated effective and even distribution of the formulations immediately after application. However, by 4 h later, significant differences emerged. The high fluidity of the free COUR 6 in the formulation might have resulted in its short residence time on the skin. As a result, its fluorescence nearly vanished after 4 h. The COUR 6-Cream group maintained significant fluorescence intensity in the epidermal layer of the skin after 4 h (Fig. 6A&B). This implied that a considerable amount of COUR 6 had not yet penetrated the deeper layers and remained in the epidermis. This retention may be related to the skin barrier function of the stratum corneum. Although the cream matrix components enable rapid drug release, they fail to enhance deep skin penetration [63]. In contrast, the COUR 6-NLC-Gel exhibited remarkable penetration capabilities. It effectively reached the dermis and subcutaneous tissue (Fig. 6A&C), demonstrating significantly high fluorescence intensity ($p < 0.01$) and a deeper penetration performance ($p < 0.01$). This result aligns with the findings of Pereira et al. [43] and Khater et al. [64]. They observed that nanoscale lipid particles were in close contact and interacted with the stratum corneum, improving

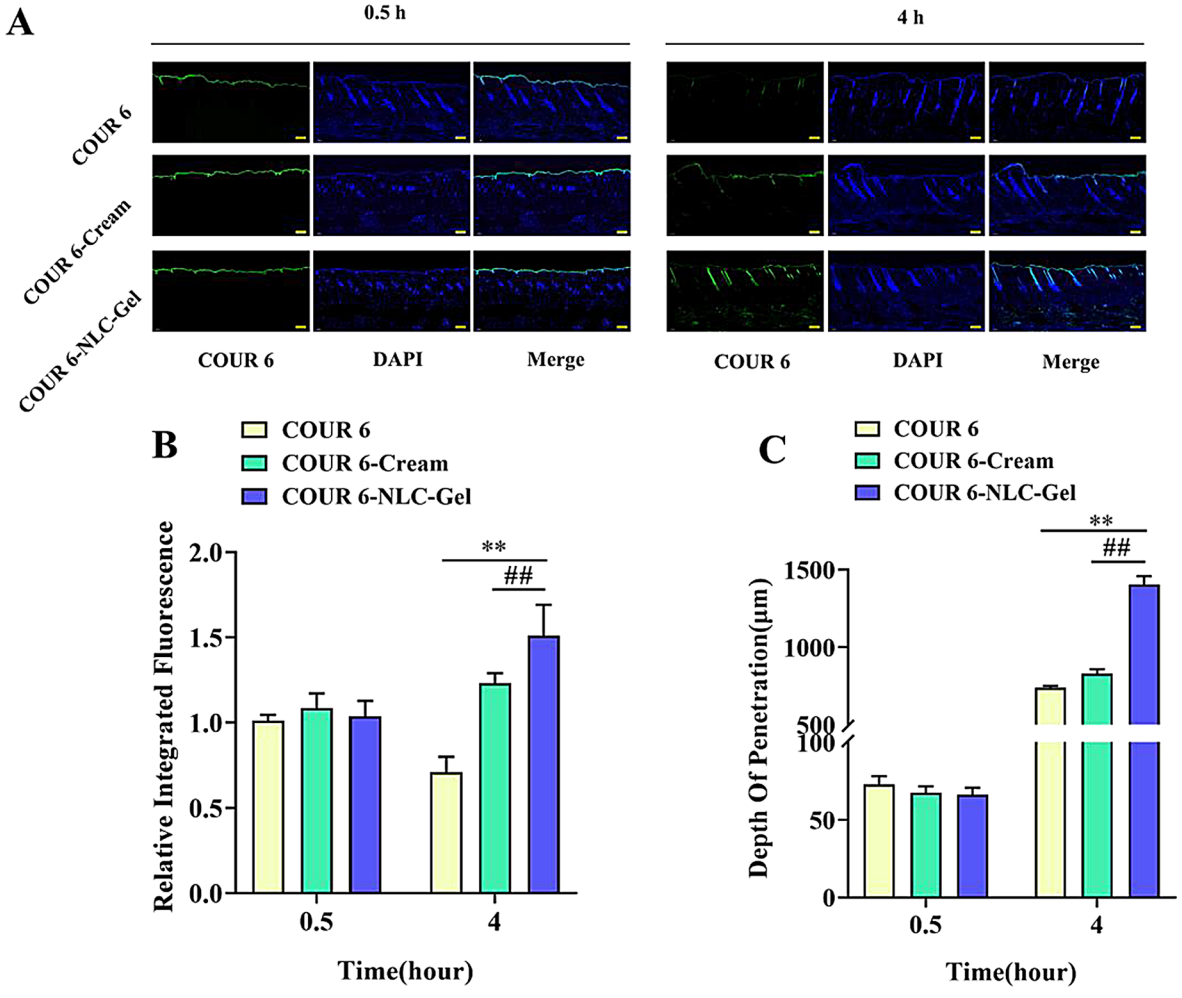


**Fig. 6** Skin permeation and distribution of COUR 6-labeled formulations. **(A)** The accumulation and penetration of COUR 6, COUR 6-Cream, and COUR 6-NLC-Gel in rat skin. Scale bar: 200 μm. **(B)** The semi-quantitative analysis of COUR 6-labeled different preparations in rats. **(C)** Skin penetration depth of different formulations labeled with COUR 6. $n = 3$, $^{**}p < 0.01$, vs. COUR 6; $^{\#\#}p < 0.01$, vs. COUR 6-Cream

drug penetration through the skin barrier for significant transdermal delivery. Furthermore, the ultra-small particle size of NLC and their hydration effect on the skin may facilitate transdermal drug absorption augmenting the transdermal penetration rate [65, 66]. Moreover, the fluorescence of COUR 6-NLC-Gel at the hair follicle sites was significantly more pronounced after local application. This observation probably resulted from the interaction between the surfactant lecithin in COUR 6-NLC-Gel and sebum, which promotes drug entry into the skin and facilitates accumulation at the hair follicle sites, thereby forming a drug reservoir [43, 67]. This finding aligns with previous research on the treatment of alopecia with minoxidil nanostructured lipid carriers [40]. Taken together, these results reveal that the NLC-Gel can facilitate the percutaneous absorption of drugs, enhance targeting efficacy, improve bioavailability, and mitigate systemic toxic side effects.

### In vitro effects of ATRA-NLC on IFN-γ-treated DPCs

To assess whether ATRA-NLC has a positive effect on the IFN-γ-induced in vitro model of AA, primary DPCs were used as experimental subjects. First, the effects of the ATRA-NLC on cell viability and proliferation were investigated. In contrast to ATRA cream-treated DPCs, ATRA-NLC-treated DPCs showed significantly increased cell viability (Fig. 7A). Flow cytometry was used to investigate the specific effects of ATRA-NLC on the DPC cell cycle (Fig. 7B). The results demonstrated that the cells in the model group were arrested in the

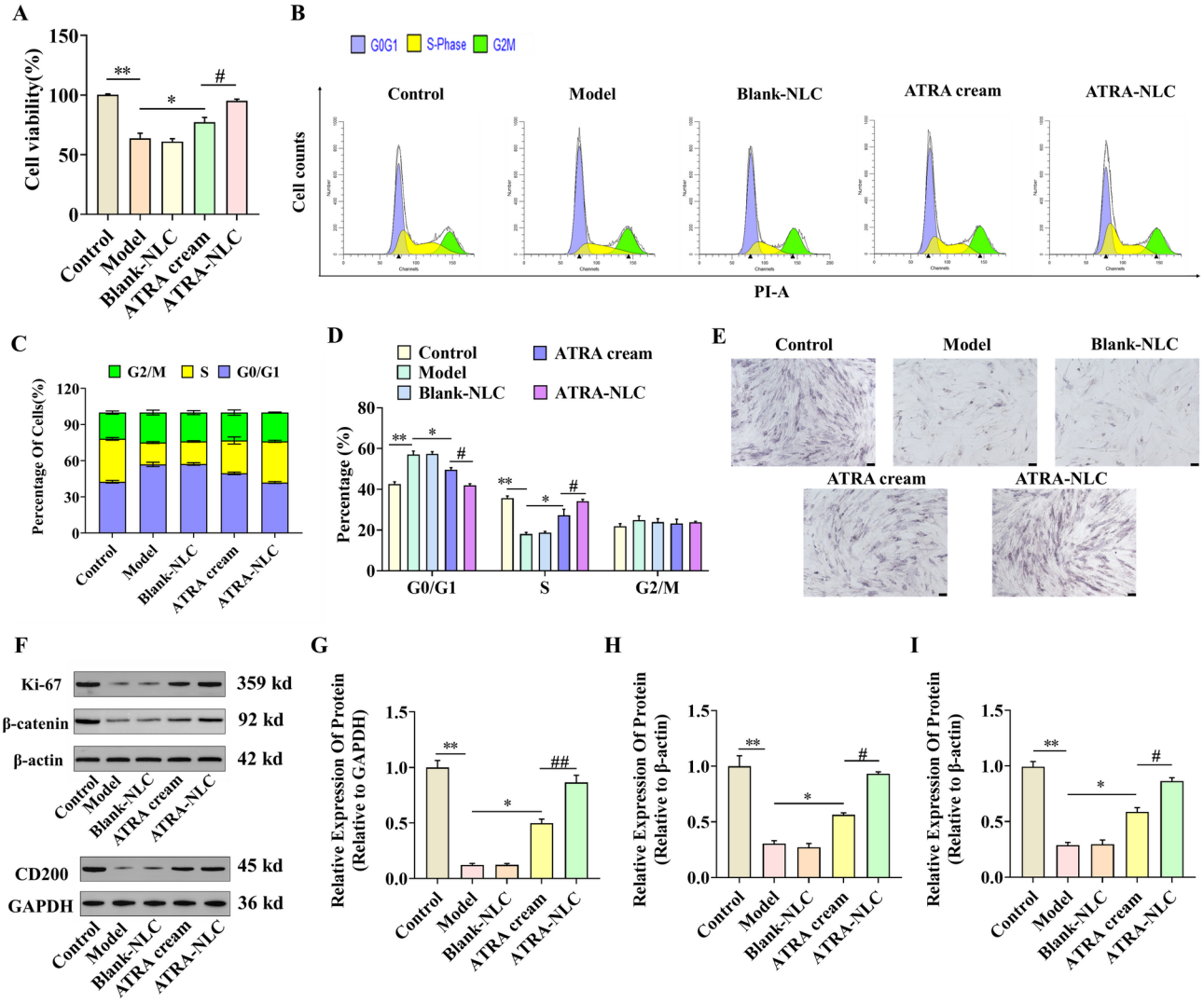


**Fig. 7** In vitro evaluationof ATRA-NLC on IFN-γ-treated DPCs. **(A)** Cell viability of different formulations on DPCs. **(B)** Cell cycle analyzed by flow cytometer. **(C, D)** Quantification of cell cycle phases. **(E)** The effect of ATRA-NLC on the activity of alkaline phosphatase (ALP) in the DPCs. Scale bar: 20 μm. **(F)** The expression levels of Ki-67, β-catenin, and CD200 were detected by Western blot. Statistical analysis of the expression levels of CD200 **(G)**, Ki-67 **(H)**, β-catenin **(I)**. n = 3, $^{*}p < 0.05$, $^{**}p < 0.01$, vs model; $^{\#}p < 0.05$, $^{\#\#}p < 0.01$, vs ATRA cream

G0/G1 phase, with a significant increase in the proportion of cells in the G0/G1 phase, suggesting that the cells might be entering a resting phase. Conversely, in the ATRA-NLC treatment group, the cell counts in the G0/G1 phase significantly decreased, while that in the S phase significantly increased, suggesting that ATRA-NLC facilitated the transition of cells from the G1 phase to the S phase and promoted the G1/S transition of the cell cycle (Fig. 7C&D). Additionally, the results of the cell viability experiment (Fig. 7A) confirmed that ATRA-NLC can promote cell proliferation, which is consistent with their regulatory effect on the cell cycle, further providing robust evidence for the proliferative effect of ATRA-NLC on cells. Cell cycle progression is a necessary condition for cell proliferation [68]. Therefore, ATRA-NLC promotes cell proliferation by regulating the cell cycle of DPCs, particularly by facilitating the G1/S transition.

Alkaline phosphatase (ALP), a pivotal marker of DPC viability, is constitutively expressed in DPCs throughout the hair growth cycle [69, 70]. Hence, the influence of different treatment groups on ALP activity in DPCs was investigated. Compared to the model group, an obvious restoration of ALP activity was observed in DPCs cultured with ATRA-NLC (Fig. 7E). This finding indicates that ATRA-NLC plays a positive role in promoting the restoration of important phenotypic characteristics of DPCs.

At present, it is widely accepted that the main pathogenic mechanism of AA resides in the breakdown of immune privilege in hair follicles [1]. CD200, an immunosuppressive factor, plays a pivotal role in hair follicles. When its expression level is abnormally low, it may precipitate the onset of androgenetic alopecia and AA [5, 71, 72]. Therefore, we performed western blotting to detect the expression of CD200. The results showed that (Fig. 7F&G) ATRA-NLC significantly restored the expression of CD200 in an in vitro AA model. Ki-67, an established marker of proliferation and morphogenesis in hair follicles, exhibits an increased expression level directly correlated with accelerated cellular proliferation within follicular cells, indicating an elevated hair growth rate [73]. Similarly, the Wnt/β-catenin signaling pathway is crucial for initiating and advancing the regenerative process of hair growth. Specifically, high levels of β-catenin in hair follicle cells can effectively accelerate the cell cycle progression, facilitating rapid hair growth [74, 75]. Based on these reports, we examined the expression profiles of these proteins. The results showed that compared to the model group, both the ATRA cream group and the ATRA-NLC group elevated the expression level of Ki-67 and β-catenin, among which the enhancement effect of the ATRA-NLC group was more pronounced ($p<0.01$) (Fig.7 F&H&I). In summary, these results demonstrate that ATRA-NLC exhibit significant advantages over ATRA cream in pharmacodynamic testing using the AA model in vitro.

### The effects of ATRA-NLC-Gel on hair regeneration in AA model mice

To verify the effect of ATRA-NLC-Gel on hair regeneration, an Imiquimod cream (IMQ)-induced AA model was employed. Mice in the model group exhibited no significant hair regeneration by Day 12, indicating the successful establishment of the AA mouse model (Fig. 8A&B). Further observations revealed that both ATRA cream and ATRA -NLC groups began showing skin pigmentation on Day 8 of treatment with visible hair regeneration on Day 12. Notably, the ATRA-NLC-Gel group demonstrated skin pigmentation as early as Day 4 of treatment, indicating the transition of hair from the telogen phase to the growth phase. As treatment continued, this group showed significant hair growth by Day 8 achieving nearly complete and dense hair coverage by Day 14, comparable to that of the control group. This indicated that the ATRA-NLC-Gel group exhibited faster and more significant effects ($p<0.01$) in promoting hair regeneration (Fig. 8C). This finding is similar to previous studies showing that tofacitinib-loaded nanostructured lipid carriers enhanced efficacy in treating alopecia areata [39]. Similar to that in the model group, no significant hair regeneration was observed in the NLC-Gel group. These results unequivocally demonstrate that the observed hair regeneration is not attributed to the carrier, but rather to the efficient delivery of ATRA via the nanostructured lipid carrier gel drug delivery system.

Hair follicle density serves as the most direct indicator reflecting the growth stages of hair. A higher hair follicle density indicates that there are more hair follicles in the anagen phase than in the telogen phase [76]. Consequently, we performed H&E staining of the skin at the application site to observe the status of the hair follicles within the skin. The hair follicles in the ATRA-NLC-Gel group penetrated deeper into the dermis, with a significant difference in density and number compared to the model group ($p<0.01$) (Fig. 8D&E). This result corresponds to the macroscopic phenomenon of hair regeneration observed in the AA model mice after treatment (Fig. 8A). The thickness of the dermis and the length of hair follicles are closely associated with the hair growth cycle [76]. As hair follicles transition from the telogen phase to the anagen phase, both dermal thickness and hair follicles length increase, whereas they decrease relatively during the telogen phase. The dermal thickness of the ATRA-NLC-Gel group was significantly different from that of the model group ($p<0.01$) (Fig. 8F). Regarding the length of hair follicles, the ATRA-NLC-Gel group exhibited a length of $273.6 \pm 17.6$ μm, while the ATRA-NLC group showed a length of $119.6 \pm 8.3$ μm. Although

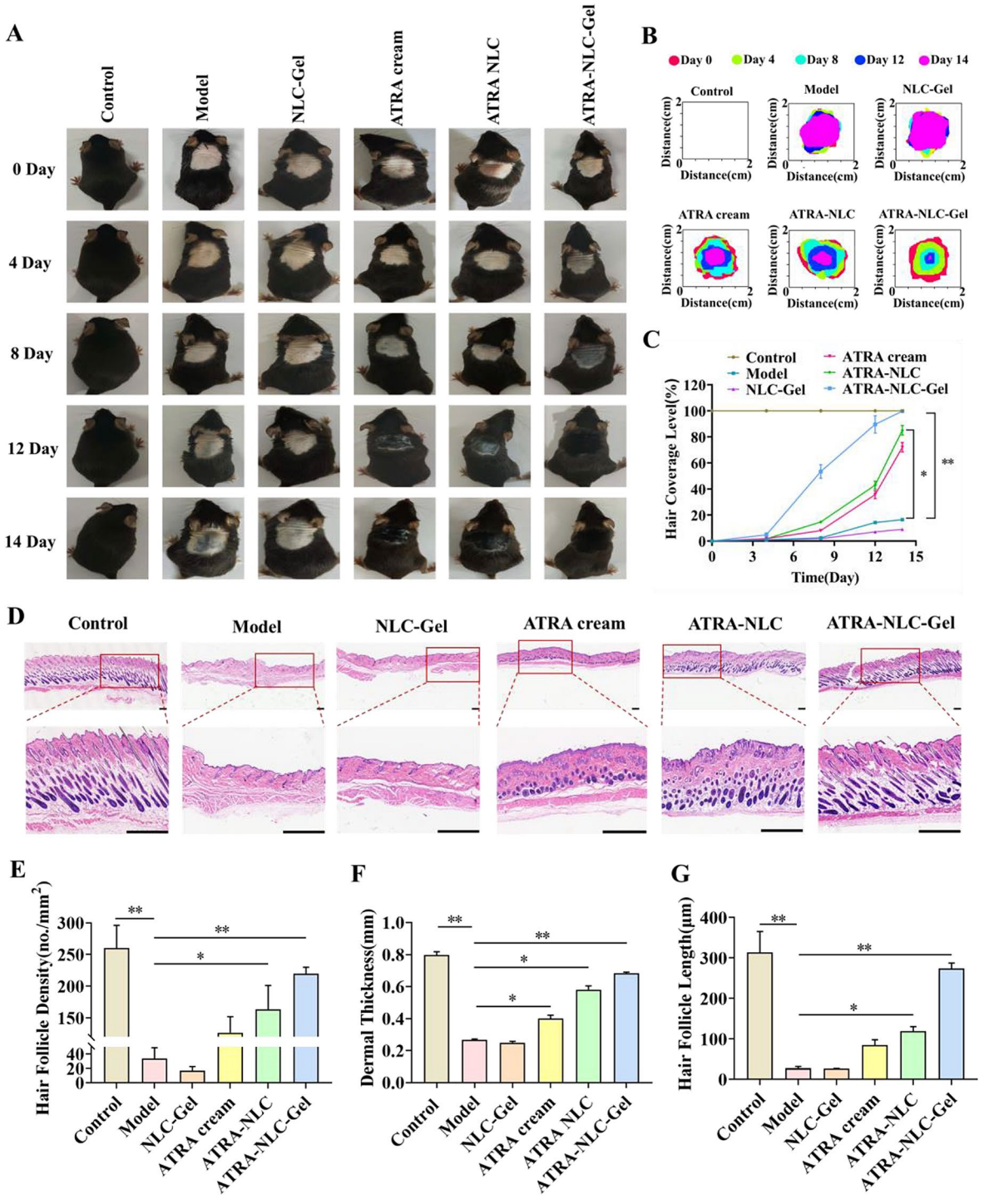


**Fig. 8** The effects of ATRA-NLC-Gel on the growth and development of hair follicles in AA model mice. **(A)** Typical images showing hair regeneration in mice from each group after drug treatment, ($n=6$). **(B)** Schematic illustration of the variation of hair loss area in each group with time. **(C)** The coverage of hair regeneration in each group at different time points, ($n=6$). **(D)** H&E staining morphology of skin hair follicles of each group after drug administration. Scale bar: 300 μm. **(E)** The density of hair follicles, the thickness of the dermis **(F)**, and the length of hair follicles **(G)** in mouse skin were measured by Image J software. $n=3$, $^{*}p<0.05$, $^{**}p<0.01$, vs. model

both groups exhibited statistically significant differences compared with the model group, the difference was more pronounced in the ATRA-NLC-Gel group (Fig. 8G). This was also reflected in the significant improvement of psoriasis-like symptoms in mice by luteolin-loaded NLC-Gel [77]. This may be attributed to the longer skin residence time of the ATRA-NLC-Gel formulation compared to that of ATRA-NLC [78], enabling sustained and slow percutaneous release (Fig. 2I), and thereby enhancing therapeutic efficacy. In summary, these results indicated that the ATRA-NLC-Gel exhibited the most effective promotion of hair regeneration in AA model mice.

#### Mechanism of ATRA-NLC-Gel in treating hair loss in AA model mice

To further explore the mechanism of action of the ATRA-NLC-Gel in treating the AA mouse model, immunofluorescence staining was employed to examine the expression location and alterations of key proteins in hair follicles and dorsal skin tissues. The results showed that the levels of Ki-67, β-catenin, and CD200 proteins in the ATRA-NLC group, and ATRA-NLC-Gel group were significantly increased ($p < 0.05$, $p < 0.01$). Notably, Ki-67 protein exhibited intense expression at the base of the hair follicle bulb in the ATRA-NLC-Gel group, whereas its expression in the other groups was relatively low (Fig. 9A). This phenomenon indicated that the ATRA-NLC-Gel promoted rapid hair regeneration in AA model mice, which aligns with the hair regeneration observed in the model mice depicted in Fig. 8A. Additionally, β-catenin and CD200 proteins were both expressed in the trunk of the hair follicle. Compared with the model group, the ATRA-NLC-Gel and ATRA-NLC groups showed significantly enhanced expression of these two proteins (Fig. 9B&C). The results of western blot experiments further confirmed that ATRA-NLC-Gel significantly upregulated the expression levels of Ki-67, β-catenin, and CD200, thereby effectively ameliorating the AA-like symptoms in mouse models (Fig. 9D-G). IFN-γ is one of the most critical factors contributing to the collapse of hair follicle immune privilege [10, 79]. TGF-β1, as an immunosuppressive molecule, is highly expressed in healthy scalps and serves as a guardian of hair follicle immune privilege [12]. Therefore, we examined the expression levels of IFN-γ and TGF-β1 in the skin. As shown in Fig. 9H&I, both ATRA-NLC and ATRA-NLC-Gel significantly downregulated the expression of IFN-γ while upregulating the expression of TGF-β1. Notably, the effects were more pronounced in the ATRA-NLC-Gel-treated group.

These results showed that, compared to the existing ATRA cream, ATRA-NLC-Gel has higher skin lipophilicity and can more effectively target hair follicles, thereby achieving stronger therapeutic effects [67]. Moreover, the significant increase in the expression levels of CD200, Ki-67, TGF-β1and β-catenin indicates that ATRA-NLC-Gel not only promotes the proliferation of hair follicle cells but also regulates the immune homeostasis of the skin [80], jointly facilitating the hair regeneration in the AA model mice.

## Conclusion

In this study, we successfully developed a nanoscale ATRA-NLC-Gel that significantly mitigated the irritative response of ATRA during transdermal delivery, markedly enhanced ATRA's skin penetration capacity and targeting efficiency to hair follicles. Furthermore, the pharmacological effects of ATRA-NLC-Gel were comprehensively evaluated using both in vitro and in vivo AA models. Pharmacological results indicated that ATRA-NLC enhanced the uptake capacity and cell cycle progression of DPCs, thereby restoring cellular activity and promoting proliferation and differentiation. When applied to the skin, ATRA-NLC-Gel can reside on the skin surface for an extended period, forming a drug reservoir that releases ATRA slowly. This allows for transdermal permeation into deeper tissues, with ATRA targeting and enriching in the hair follicles. The formulation modulated the expression of relevant cytokines and proteins, thereby promoting hair follicle growth and development to a certain extent, restoring the immune privilege of hair follicles, and significantly promoting hair regrowth in the AA mouse model. These findings suggest that ATRA-NLC-Gel provides a novel scientific basis and practical reference for the clinical treatment of AA.

## Materials and methods

The materials, animals, and cells are described in S1 Materials and S2 Cells and Animals in Supplementary Material 1.

#### Preparation and characterization of ATRA-NLC

The ATRA-NLC was prepared by the ultrasonic emulsification [81]. Briefly, 80 mg of GMS and 320 μL of IM containing 12.5 mg of ATRA were melted and mixed uniformly at 85 °C to form the lipid phase. This solution was then combined with 10 mL of an aqueous phase containing 2.5% lecithin also maintained at 85 °C. The mixture was emulsified by stirring at 2500 rpm for 10 min to form the primary emulsion. Following an additional 8 min of ultrasonic treatment, centrifugal separation was performed to remove the free ATRA, ultimately yielding ATRA-NLC. Using the steps outlined above, blank nanoparticles without ATRA were also prepared as a control. To prepare the COUR 6-loaded nanoparticles, COUR 6 was used in replacement of ATRA at the same concentration. And the experimental approach for the

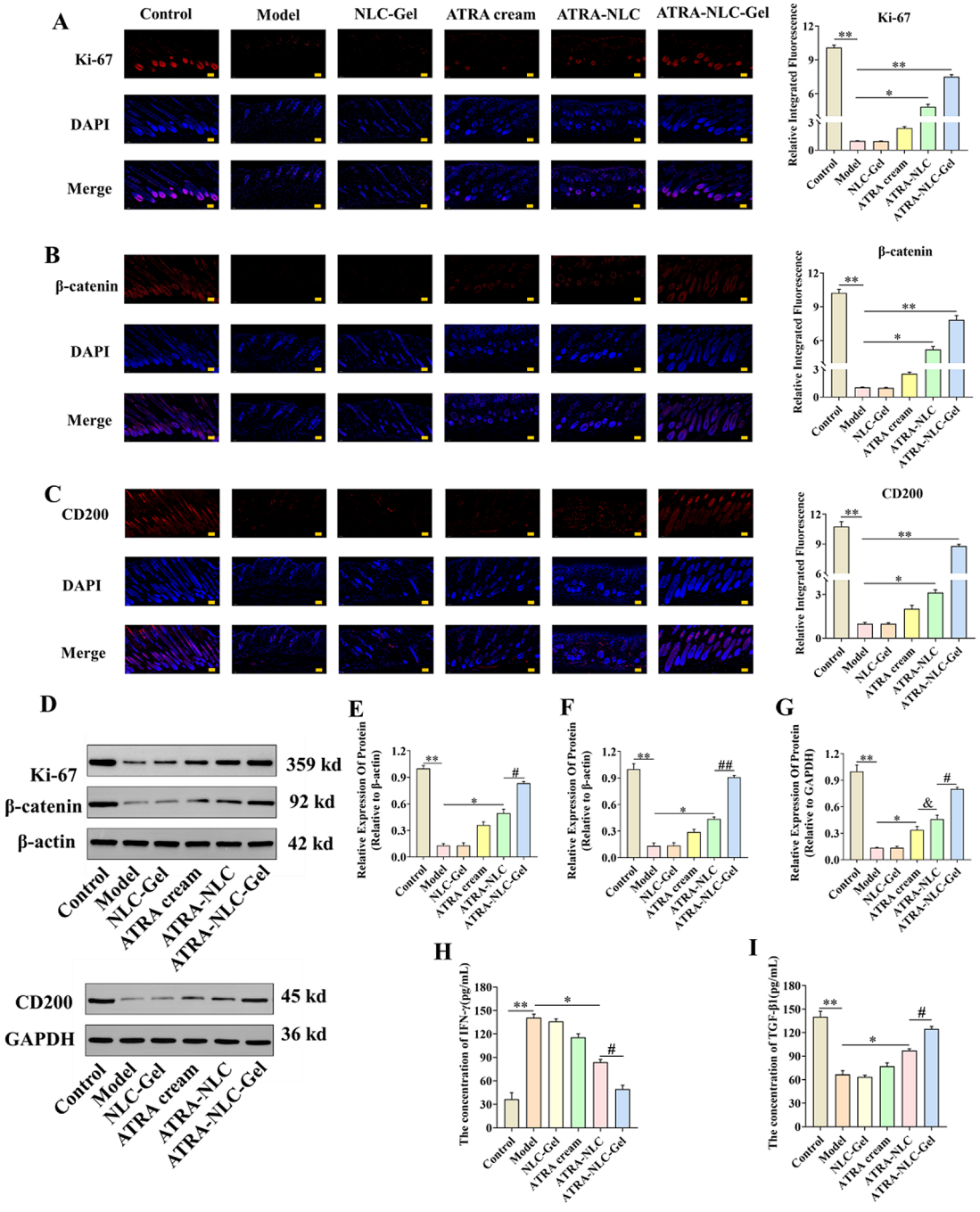


**Fig. 9** Mechanism of ATRA-NLC-Gel in treating hair loss in AA model mice. Immunofluorescence of Ki-67 **(A)**, β-catenin **(B)**, and CD200 **(C)** on skin samples from different treatment groups. Scale bars: 100 μm. **(D)** The expression levels of Ki-67, β-catenin, and CD200 were detected by Western blot. Statistical analysis of the expression levels of Ki-67 **(E)**, β-catenin **(F)**, CD200 **(G)**. The expression levels of IFN-γ**(H)** and TGF-β1**(I)** were determined by ELISA in skin tissue. $n = 3$, $^{*}p < 0.05$, $^{**}p < 0.01$,vs. model; $^{\#}p < 0.05$, $^{\#\#}p < 0.01$, vs. ATRA-NLC; $^{\&}p < 0.05$, vs. ATRA cream

preparation of COUR 6-Cream has been incorporated in Supplementary Material S3.

The morphology of the nanoparticles was observed using TEM, and a Zetasizer Nano ZSE system was employed to measure the zeta potential, particle size and PDI (the methods are detailed in Supplementary Material 4&5). The FT-IR spectra of Blank-NLC, ATRA-NLC, and ATRA were recorded using a Nicolet iS50 FT-IR spectrometer (Thermo Scientific, MA, USA) within the wavenumber range of 4000–500 $cm^{-1}$. And the method for DSC analysis is detailed in Supplementary Material S6.

The amount of ATRA was measured using high-performance liquid chromatography (HPLC; Shimadzu, Japan). The specific measurement conditions and methods are

detailed in Supplementary Material S7. The drug-loading (DL) and encapsulation efficiency (EE) were determined using Eqs. 1 and 2, respectively.

$$DL\ (\%) = \frac{(\text{Total ATRA} - \text{free ATRA})}{\text{Total ATRA} - \text{NLC}} \times 100\% \quad (1)$$

$$\text{EE}\ (\%) = \frac{(\text{Total ATRA} - \text{free ATRA})}{\text{Total ATRA}} \times 100\% \quad (2)$$

#### Preparation and characterization of ATRA-NLC-Gel

The blank gel was prepared by dissolving carbomer 940 (0.6%, w/v), glycerin (10%, v/v), sodium bisulfite (0.1%, w/v), and L-menthol (0.1%, w/v) in distilled water. The pH of the system was adjusted to 6.5 by adding an appropriate amount of triethanolamine. Subsequently, the prepared blank gel was combined with ATRA-NLC at a ratio of 4:1(w/v) to form an ATRA-NLC-Gel containing ATRA at a concentration of 0.025%. Similarly, Blank-NLC was incorporated into the blank gel to yield NLC-Gel. The internal structure and morphology of the ATRA-NLC-Gel were investigated using a Cryogenic Scanning Electron Microscope (Hitachi Regulus 8100, Japan), the methods are detailed in Supplementary Material S8.

#### In vitro release of ATRA-NLC and ATRA-NLC-Gel

The in vitro drug release behavior of different ATRA formulations was analyzed using the dialysis method [59, 82]. Briefly, a fixed amount of free ATRA, ATRA cream, ATRA-NLC, and ATRA-NLC-Gel was placed in dialysis bags (MWCO 10 KDa), which were subsequently submerged in the release medium (ethanol: PBS, v/v, 3:7). At 37 °C, the medium was stirred at a constant speed of 120 rpm. At predetermined intervals (0.5, 2, 4, 8, 12, 24, and 48 h), 200 μL samples of the release solution were taken and immediately replenished with an equal volume of fresh medium. The ATRA concentration in the released solution was analyzed using HPLC. The cumulative release rate of ATRA from various formulations was computed as follows:

$$\mathrm{Q_n} = \mathrm{V_0 C_n} + \mathrm{V} \sum \mathrm{C_i} \quad (3)$$

$$\text{Cumulative release rate}\ (\%) = \frac{\mathrm{Q_n}}{\mathrm{Q_{total}}} \times 100\% \quad (4)$$

Where $Q_n$ represents the cumulative amount of ATRA released from the formulation at the $n^{th}$ sampling point. $Q_{total}$ denotes the total content of ATRA in the formulation, where $C_n$ indicates the concentration of ATRA in the release medium at the $n^{th}$ sampling point. ΣCi denotes the summation of the concentrations of the drug in the release medium at all sampling instants from the first sampling time point to the i-th sampling time point. V refers to the volume of the released liquid extracted each time, $V_0$ is the overall volume of the release medium.

#### Evaluation of stability

In accordance with ICH Guideline Q1A(R2) (2003), the stability study of ATRA-NLC-Gel was conducted at 4 °C and 25 °C [55, 83]. This research involved five months of continuous observation, assessing the stability by visually inspecting the changes in the appearance and morphology of the samples, as well as by monitoring the particle size and PDI of ATRA-NLC in ATRA-NLC-Gel, and the content variation of ATRA was calculated with Eq. 5.

$$\text{ATRA Content}\ (\%) = \left(1 - \frac{\text{Total loss of ATRA}}{\text{Total mass of ATRA in ATRA} - \text{NLC} - \text{Gel}}\right) \times 100\% \quad (5)$$

#### In vitro and in vivo biosafety assessment

The in vitro biological safety was evaluated by detecting the cytotoxicity of ATRA cream, ATRA-NLC and ATRA-NLC-Gel using the CCK-8 assay kit [84]. DPCs were seeded at a density of $1 \times 10^4$ cells per well in a 96-well plate and cultured under standard cell culture conditions for 24 h. Subsequently, ATRA cream, ATRA-NLC and ATRA-NLC-Gel were introduced at concentrations ranging from 0.2 to 1 μg/mL, and the cells were incubated for an additional 24 h. Following this, 100 μL of CCK-8 solution (be diluted tenfold) was added to each well, and the cells were incubated for 1 h. Finally, absorbance was measured at 450 nm using a Microplate Reader (Thermo Fisher Scientific, USA).

Multiple skin irritation experiments were carried out in reference to OECD Test Guideline 404 to assess the in vivo toxicity of ATRA-NLC-Gel [85]. The dorsal skin of male SD rats was divided into four regions. Physiological saline and ATRA alcohol solution (20 μL/cm²), as well as ATRA-NLC-Gel and ATRA ointment (20 mg/cm²), all with an ATRA concentration of 0.025%, were applied to the rat's dorsal skin once daily for 14 days. Skin reactions such as erythema, eschar, and edema were scored according to a scoring system [59], as shown in Table S1. Skin irritation results were used to assess in vivo biosafety. The study protocol received approval from the Institutional Animal Care and Use Committee and was carried out in compliance with the guidelines for animal experimentation established by the Air Force Medical University.

#### Cellular uptake

DPCs were inoculated at a density of $3 \times 10^5$ cells per well and cultured for 24 h. Free COUR 6, COUR 6-Cream, and COUR 6-NLC were prepared at a concentration of 1 μM for 0.5, 1.5, and 3 h. Post-incubation, cells were

washed thrice with PBS (5 min), fixed with paraformaldehyde (15 min), stained with DAPI (10 min), and observations were finally made via a CLSM. Cells were seeded in six-well plates at the same density and processed identically. Subsequently, cell uptake was quantitatively analyzed using a flow cytometer (FCM, Beckman Coulter, USA) [86].

#### In vivo skin distribution

The penetration and distribution of the different formulations in the skin were studied using CLSM. In brief, after treatment with COUR 6 (20 μL/cm²), COUR 6-Cream and COUR 6-NLC-Gel onto the skin of SD rats (20 mg/cm²), with the final concentration of COUR 6 set at 0.025%. the rats were kept in the dark. Frozen sections of skin tissue were collected at 0.5 h and 4 h post-administration, and subsequently scanned for observation [59].

#### DPCs viability assessment

Based on previous literature reports, an in vitro AA model was established by co-incubating cells with IFN-γ at a concentration of 100 ng/mL for 48 h [87]. Following the successful establishment of an in vitro AA model, DPCs were treated with Blank-NLC, ATRA cream, and ATRA-NLC, with the final concentration of ATRA set at 0.6 μg/mL. Subsequently, the cell viability was assessed using a CCK-8 kit 24 h after the cells were treated.

#### Flow cytometry analysis of the cell cycle

Following cell culture and modeling, the cells were treated with different drugs for an additional 24 h before being transferred to collection tubes. Subsequently, the cells were fixed overnight at 4 °C in 1 mL of cold fixative solution (anhydrous ethanol: PBS, 7:3). Thereafter, the cells were thrice washed with cold PBS and resuspended in PI/RNase staining buffer (0.5 mL), followed by incubation in the dark for 30 min. Finally, the cell cycle distribution was determined via FCM [88].

#### ALP staining

For ALP staining, DPCs were seeded in a 12-well culture plate, modeled, and incubated with different drugs for 24 h. The cells were then washed twice with cold PBS and fixed in 4% paraformaldehyde at room temperature for 15 min. Subsequently, the cells were incubated in the presence of a BCIP/NBT alkaline phosphatase chromogenic solution. A deep purple color indicates a positive ALP signal [70].

#### Establishment and drug administration of animal models for AA

Referring to previous studies on the establishment of an IMQ-induced AA model [39]. The dorsal skin of the mice began to lose hair and presented with an area of alopecia greater than 1 cm², indicating that the AA model had been successfully established. The mice were then randomly divided into six groups: Control, Model, NLC-Gel, ATRA cream, ATRA-NLC, and ATRA-NLC-Gel, with six mice in each group. Different formulations were applied topically to the alopecic areas once daily for 14 days (ATRA-NLC 4 μL/cm²/mouse, ointment 20 mg/cm²/mouse). During the treatment period, photographs were taken to detect hair regeneration on the dorsal skin of mice, and hair density was analyzed using ImageJ software.

#### H&E staining

After drug administration, mice were euthanized using isoflurane. Skin tissue at the treatment site was isolated and fixed in 4% paraformaldehyde. Following fixation, routine paraffin embedding and sectioning were conducted, followed by hematoxylin and eosin staining. Finally, the sections were mounted, observed and photographed using an inverted microscope.

#### Detection of cytokines by ELISA

For detailed information, please refer to Supplementary Material S9.

#### Immunofluorescence

Skin tissues were excised and fixed in 4% formaldehyde solution for 24 h, followed by embedding in paraffin for sectioning. Immunostaining was performed using the Ki-67 antibody (Servicebio, GB121142,1:200), β-catenin antibody (Servicebio, GB15003,1:200), and CD200 antibody (Abcam, ab314662,1:100). Following incubation with primary and secondary antibodies, the DAPI working solution was added. After sealing the coverslips, observation, and image acquisition were conducted using a fluorescence microscope.

#### Western blot analysis

Following the previously established method [84], western blot analysis was performed. The membranes were incubated overnight at 4 °C with the primary antibodies against.

CD200 (Abcam, ab314662, 1:1000), β-catenin (Servicebio, GB150016, 1:1000), Ki-67 (Servicebio, GB121142, 1:1000), β-actin (Servicebio, GB15003, 1:2000), and GAPDH (Servicebio, GB15004, 1:3000). After washing the membranes thrice with PBST, they were incubated with secondary antibodies at room temperature for 1 h. The membranes were washed again with PBST and the proteins were visualized using a gel imaging system (Bio-Rad, USA).

### Statistical analysis

Data were analyzed using GraphPad Prism 8.3 software and presented as Mean ± SD. Statistical comparisons between different groups were made using one-way ANOVA. In the stability assessment of the ATRA-NLC-Gel, repeated measures ANOVA was used for statistical analysis between two groups. With $p < 0.05$ considered to indicate a statistically significant difference.

## Supplementary Information

The online version contains supplementary material available at https://doi.org/10.1186/s12951-025-03407-w.

Supplementary Material 1

Supplementary Material 2

#### Author contributions

The whole study was conceived and designed by JWW, DX, YW and LL Zheng. LL Zheng conducted the primary experiments, carried out data analysis. LL Zheng and DX prepared the initial draft of the manuscript. YD, LL Zhang, FXJ supported experiments and data analysis. WTL, XZ, YPY provided valuable suggestions and reviewed the manuscript. All authors have reviewed and approved the final version of the article.

#### Funding

This research received financial support from the Clinical Medicine and Pharmacy Research Center of Air Force Medical University (LHJJ2024-YX03), as well as from the Xijing Hospital Project for Enhancing the Training of Medical Staff (XJZT24CZ14, XJZT25QN56), and the Talent Project established by Chinese Pharmaceutical Association Hospital Phamacy department (NO. CPA-Z05-ZC-2022-003), the Innovation Capacity Support Program of Shaanxi Province (2023-CX-TD-76), and the Health Research and Innovation Capacity Enhancement Program of Shaanxi Province (2023 PT-10).

#### Data availability

No datasets were generated or analysed during the current study.

## Declarations

#### Ethics approval and consent to participate

All procedures were approved by the Animal Ethics Committee of Air Force Medical University, and were conducted in accordance with the regulations outlined in the Guide for the Care and Use of Laboratory Animals. The license number of the animals is No. IACUC-20241326.

#### Competing interests

The authors declare no competing interests.

#### Author details

[1]Department of Pharmacy, Xijing Hospital, Air Force Medical University, Xi'an 710032, China
[2]Department of Pharmacy, The First Affiliated Hospital of Army Medical University, Chongqing 400038, China
[3]Department of Pharmacology, Shaanxi University of Chinese Medicine, Xianyang 712046, China
[4]College of Life Sciences, Northwest University, Xi'an 710069, China

Received: 8 January 2025 / Accepted: 19 April 2025
Published online: 16 May 2025

#### References

1. Pratt CH, King LE, Messenger AG, Christiano AM, Sundberg JP. Alopecia areata. Nat Reviews Disease Primers 2017, 3.
2. Lee HH, Gwillim E, Patel KR, Hua T, Rastogi S, Ibler E, Silverberg JI. Epidemiology of alopecia areata, ophiasis, totalis, and universalis: A systematic review and meta-analysis. J Am Acad Dermatol. 2020;82:675–82.
3. de Lusignan S, Alexander H, Broderick C, Dennis J, McGovern A, Feeney C, Flohr C. Atopic dermatitis and risk of autoimmune conditions: Population-based cohort study. J Allergy Clin Immunol. 2022;150:709–13.
4. Barton VR, Toussi A, Awasthi S, Kiuru M. Treatment of pediatric alopecia areata: A systematic review. J Am Acad Dermatol. 2022;86:1318–34.
5. Bertolini M, McElwee K, Gilhar A, Bulfone-Paus S, Paus R. Hair follicle immune privilege and its collapse in alopecia areata. Exp Dermatol. 2020;29:703–25.
6. Redler S, Angisch M, Heilmann S, Wolf S, Barth S, Basmanav BF, Giehl KA, Hanneken S, Eigelshoven S, Mangold E, et al. Immunochip-based analysis: high-density genotyping of immune-related loci sheds further light on the autoimmune genetic architecture of alopecia areata. J Invest Dermatol. 2015;135:919–21.
7. Jeon JJ, Jung SW, Kim YH, Parisi R, Lee JY, Kim MH, Lee WS, Lee S. Global, regional and National epidemiology of alopecia areata: a systematic review and modelling study. Br J Dermatol. 2024;191:325–35.
8. Villasante Fricke AC, Miteva M. Epidemiology and burden of alopecia areata: a systematic review. Clin Cosmet Investig Dermatol. 2015;8:397–403.
9. Gilhar A, Etzioni A, Paus R. Alopecia areata. N Engl J Med. 2012;366:1515–25.
10. McElwee KJ, Gilhar A, Tobin DJ, Ramot Y, Sundberg JP, Nakamura M, Bertolini M, Inui S, Tokura Y, King LE Jr., et al. What causes alopecia areata? Exp Dermatol. 2013;22:609–26.
11. Meyer KC, Klatte JE, Dinh HV, Harries MJ, Reithmayer K, Meyer W, Sinclair R, Paus R. Evidence that the Bulge region is a site of relative immune privilege in human hair follicles. Br J Dermatol. 2008;159:1077–85.
12. Foitzik K, Lindner G, Mueller-Roever S, Maurer M, Botchkareva N, Botchkarev V, Handjiski B, Metz M, Hibino T, Soma T, et al. Control of murine hair follicle regression (catagen) by TGF-beta1 in vivo. Faseb J. 2000;14:752–60.
13. Ashrafuzzaman M, Yamamoto T, Shibata N, Hirayama TT, Kobayashi M. Potential involvement of the stem cell factor receptor c-kit in alopecia areata and androgenetic alopecia: histopathological, immunohistochemical, and semiquantitative investigations. Acta Histochem Cytochem. 2010;43:9–17.
14. Liu Z, Liu X. Gut microbiome, metabolome and alopecia areata. Front Microbiol. 2023;14:1281660.
15. Joly P, Lafon A, Houivet E, Donnadieu N, Richard MA, Dupuy A, Delaporte E, Bernard P, Machet L, Tosti A, et al. Efficacy of methotrexate alone vs methotrexate plus Low-Dose prednisone in patients with alopecia areata totalis or universalis: A 2-Step Double-Blind randomized clinical trial. JAMA Dermatol. 2023;159:403–10.
16. Stoehr JR, Choi JN, Colavincenzo M, Vanderweil S. Off-Label use of topical Minoxidil in alopecia: A review. Am J Clin Dermatol. 2019;20:237–50.
17. King BA, Craiglow BG. Janus kinase inhibitors for alopecia areata. J Am Acad Dermatol. 2023;89:S29–32.
18. Civas E, Aksoy B, Ozer F, Eski M. Long-term result of hair transplantation for therapy resistant alopecia areata of eyebrows. Indian J Dermatol Venereol Leprol. 2017;83:618–9.
19. Younis N, Puigmal N, Kurdi AE, Badaoui A, Zhang D, Morales-Garay C, Saad A, Cruz D, Rahy NA, Daccache A, et al. Microneedle-Mediated delivery of immunomodulators restores immune privilege in hair follicles and reverses immune-Mediated alopecia. Adv Mater. 2024;36:e2312088.
20. Demetriou AA, Levenson SM, Rettura G, Seifter E. Vitamin A and retinoic acid: induced fibroblast differentiation in vitro. Surgery. 1985;98:931–4.
21. Lu KJ, Wang W, Xu XL, Jin FY, Qi J, Wang XJ, Kang XQ, Zhu ML, Huang QL, Yu CH, et al. A dual deformable liposomal ointment functionalized with retinoic acid and epidermal growth factor for enhanced burn wound healing therapy. Biomater Sci. 2019;7:2372–82.
22. Orfanos CE, Zouboulis CC, Almond-Roesler B, Geilen CC. Current use and future potential role of retinoids in dermatology. Drugs. 1997;53:358–88.
23. Bazzano. GS. N T, W G: <topical for="growth=" hair="promotion.pdf=" tretinoin=""></topical>. J Am Acad Dermatol 1986.
24. Wen L, Fan Z, Huang W, Miao Y, Zhang J, Liu B, Zhu D, Dai D, Zhang J, Le D et al. Retinoic acid drives hair follicle stem cell activation via Wnt/β-catenin signalling in androgenetic alopecia. J Eur Acad Dermatol Venereol 2024.
25. Tierney MT, Polak L, Yang Y, Abdusselamoglu MD, Baek I, Stewart KS, Fuchs E. Vitamin A resolves lineage plasticity to orchestrate stem cell lineage choices. Science. 2024;383:eadi7342.
26. Li A, He M, Wang H, Qiao B, Chen P, Gu H, Zhang M, He S. All-trans retinoic acid negatively regulates cytotoxic activities of nature killer cell line 92. Biochem Biophys Res Commun. 2007;352:42–7.

27. Szuts EZ, Harosi FI. Solubility of retinoids in water. Arch Biochem Biophys. 1991;287:297–304.
28. Lin HS, Chean CS, Ng YY, Chan SY, Ho PC. 2-hydroxypropyl-beta-cyclodextrin increases aqueous solubility and photostability of all-trans-retinoic acid. J Clin Pharm Ther. 2000;25:265–9.
29. Rahman SA, Abdelmalak NS, Badawi A, Elbayoumy T, Sabry N, El Ramly A. Formulation of tretinoin-loaded topical proniosomes for treatment of acne: in-vitro characterization, skin irritation test and comparative clinical study. Drug Deliv. 2015;22:731–9.
30. Gordillo-Galeano A, Mora-Huertas CE. Solid lipid nanoparticles and nanostructured lipid carriers: A review emphasizing on particle structure and drug release. Eur J Pharm Biopharm. 2018;133:285–308.
31. Okonogi S, Riangjanapatee P. Physicochemical characterization of lycopene-loaded nanostructured lipid carrier formulations for topical administration. Int J Pharm. 2015;478:726–35.
32. Krambeck K, Silva V, Silva R, Fernandes C, Cagide F, Borges F, Santos D, Otero-Espinar F, Lobo JMS, Amaral MH. Design and characterization of nanostructured lipid carriers (NLC) and nanostructured lipid carrier-based hydrogels containing Passiflora edulis seeds oil. Int J Pharm. 2021;600:120444.
33. Lalan M, Shah P, Shah K, Prasad A. Developmental studies of Curcumin NLCs as safe alternative in management of infectious childhood dermatitis. Nanosci Nanotechnology-Asia. 2020;10:390–403.
34. Patel VN, Patel HV, Agrawal K, Soni I, Shah P, Mangrulkar SV, Umekar MJ, Lalan MS. Comprehensive developmental investigation on Simvastatin enriched bioactive film forming spray using the quality by design paradigm: a prospective strategy for improved wound healing. J Drug Target. 2024;32:1139–53.
35. Puglia C, Bonina F. Lipid nanoparticles as novel delivery systems for cosmetics and dermal pharmaceuticals. Expert Opin Drug Deliv. 2012;9:429–41.
36. Borderwala K, Swain G, Mange N, Gandhi J, Lalan M, Singhvi G, Shah P. Optimization of solid lipid nanoparticles of Ezetimibe in combination with Simvastatin using quality by design (QbD). Nanosci Nanotechnology-Asia. 2020;10:404–18.
37. Mittal A, Schulze K, Ebensen T, Weissmann S, Hansen S, Guzmán CA, Lehr CM. Inverse micellar sugar glass (IMSG) nanoparticles for transfollicular vaccination. J Control Release. 2015;206:140–52.
38. Lin YK, Al-Suwayeh SA, Leu YL, Shen FM, Fang JY. Squalene-containing nanostructured lipid carriers promote percutaneous absorption and hair follicle targeting of diphencyprone for treating alopecia areata. Pharm Res. 2013;30:435–46.
39. Li Q, Wang Y, Guo Q, Cao J, Feng Y, Ke X. Nanostructured lipid carriers promote percutaneous absorption and hair follicle targeting of Tofacitinib for treating alopecia areata. J Controlled Release. 2024;372:778–94.
40. Oliveira PM, Alencar-Silva T, Pires FQ, Cunha-Filho M, Gratieri T, Carvalho JL, Gelfuso GM. Nanostructured lipid carriers loaded with an association of Minoxidil and Latanoprost for targeted topical therapy of alopecia. Eur J Pharm Biopharm. 2022;172:78–88.
41. Doktorovova S, Souto EB. Nanostructured lipid carrier-based hydrogel formulations for drug delivery: a comprehensive review. Expert Opin Drug Deliv. 2009;6:165–76.
42. Angelo T, El-Sayed N, Jurisic M, Koenneke A, Gelfuso GM, Cunha-Filho M, Taveira SF, Lemor R, Schneider M, Gratieri T. Effect of physical stimuli on hair follicle deposition of clobetasol-loaded lipid nanocarriers. Sci Rep. 2020;10:176.
43. Pereira MN, Tolentino S, Pires FQ, Anjos JLV, Alonso A, Gratieri T, Cunha-Filho M, Gelfuso GM. Nanostructured lipid carriers for hair follicle-targeted delivery of clindamycin and rifampicin to hidradenitis suppurativa treatment. Colloids Surf B 2021, 197.
44. Santos GA, Angelo T, Andrade LM, Silva SMM, Magalhães PO, Cunha-Filho M, Gelfuso GM, Taveira SF, Gratieri T. The role of formulation and follicular pathway in voriconazole cutaneous delivery from liposomes and nanostructured lipid carriers. Colloids Surf B Biointerfaces. 2018;170:341–6.
45. Silva LA, Andrade LM, de Sá FA, Marreto RN, Lima EM, Gratieri T, Taveira SF. Clobetasol-loaded nanostructured lipid carriers for epidermal targeting. J Pharm Pharmacol. 2016;68:742–50.
46. Maulvi FA, Lakdawala DH, Shaikh AA, Desai AR, Choksi HH, Vaidya RJ, Ranch KM, Koli AR, Vyas BA, Shah DO. In vitro and in vivo evaluation of novel implantation technology in hydrogel contact lenses for controlled drug delivery. J Control Release. 2016;226:47–56.
47. Sikora A, Shard AG, Minelli C. Size and ζ-Potential measurement of silica nanoparticles in serum using tunable resistive pulse sensing. Langmuir. 2016;32:2216–24.
48. Kesharwani P, Md S, Alhakamy NA, Hosny KM, Haque A. QbD Enabled Azacitidine Loaded Liposomal Nanoformulation and Its In Vitro Evaluation. Polymers 2021, 13.
49. Agrawal Y, Petkar KC, Sawant KK. Development, evaluation and clinical studies of acitretin loaded nanostructured lipid carriers for topical treatment of psoriasis. Int J Pharm. 2010;401:93–102.
50. Xu D, Qiao T, Wang Y, Wang Q-S, Cui Y-L. Alginate nanogels-based thermosensitive hydrogel to improve antidepressant-like effects of Albiflorin via intranasal delivery. Drug Delivery. 2021;28:2137–49.
51. Al Harthi S, Alavi SE, Radwan MA, El Khatib MM, AlSarra IA. Nasal delivery of donepezil HCl-loaded hydrogels for the treatment of Alzheimer's disease. Sci Rep. 2019;9:9563.
52. Ghanbarzadeh S, Hariri R, Kouhsoltani M, Shokri J, Javadzadeh Y, Hamishehkar H. Enhanced stability and dermal delivery of hydroquinone using solid lipid nanoparticles. Colloids Surf B Biointerfaces. 2015;136:1004–10.
53. Hu X, Wei W, Qi X, Yu H, Feng L, Li J, Wang S, Zhang J, Dong W. Preparation and characterization of a novel pH-sensitive Salecan-g-poly(acrylic acid) hydrogel for controlled release of doxorubicin. J Mater Chem B. 2015;3:2685–97.
54. Yamaguchi Y, Nagasawa T, Nakamura N, Takenaga M, Mizoguchi M, Kawai S, Mizushima Y, Igarashi R. Successful treatment of photo-damaged skin of nano-scale AtRA particles using a novel transdermal delivery. J Control Release. 2005;104:29–40.
55. Diaz DA, Lynch M, McMahon M, Oblessuc R, Colgan ST. Science and Risked-Based stability testing Strategies-a test case on the global implementation and regulatory reception. Aaps J. 2020;22:140.
56. Zhang P, Kling RE, Ravuri SK, Kokai LE, Rubin JP, Chai JK, Marra KG. A review of adipocyte lineage cells and dermal papilla cells in hair follicle regeneration. J Tissue Eng. 2014;5:2041731414556850.
57. Han F, Yin R, Che X, Yuan J, Cui Y, Yin H, Li S. Nanostructured lipid carriers (NLC) based topical gel of flurbiprofen: design, characterization and in vivo evaluation. Int J Pharm. 2012;439:349–57.
58. Weckel A, Dhariwala MO, Ly K, Tran VM, Ojewumi OT, Riggs JB, Gonzalez JR, Dwyer LR, Okoro JN, Leech JM, et al. Long-term tolerance to skin commensals is established neonatally through a specialized dendritic cell subgroup. Immunity. 2023;56:1239–e12541237.
59. Wang W, Shu GF, Lu KJ, Xu XL, Sun MC, Qi J, Huang QL, Tan WQ, Du YZ. Flexible liposomal gel dual-loaded with all-trans retinoic acid and betamethasone for enhanced therapeutic efficiency of psoriasis. J Nanobiotechnol. 2020;18:80.
60. Inokuchi Y, Hironaka K, Fujisawa T, Tozuka Y, Tsuruma K, Shimazawa M, Takeuchi H, Hara H. Physicochemical properties affecting retinal Drug/Coumarin-6 delivery from nanocarrier systems via Eyedrop administration. Investig Ophthalmol Vis Sci. 2010;51:3162–70.
61. Pretor S, Bartels J, Lorenz T, Dahl K, Finke JH, Peterat G, Krull R, Al-Halhouli AT, Dietzel A, Büttgenbach S, et al. Cellular uptake of coumarin-6 under microfluidic conditions into HCE-T cells from nanoscale formulations. Mol Pharm. 2015;12:34–45.
62. <A study on the role of zwitterionic phosphatidylcholine lipid (s) in physicochemical features of liposome encapsulated paclitaxel as a drug delivery system.pdf>.
63. Kim M-H, Kim K-T, Sohn S-Y, Lee J-Y, Lee CH, Yang H, Lee BK, Lee KW, Kim D-D.: formulation and evaluation of nanostructured lipid carriers (NLCs) of 20(S)-Protopanaxadiol (PPD) by Box-Behnken design. Int J Nanomed. 2019;14:8509–20.
64. Khater D, Nsairat H, Odeh F, Saleh M, Jaber A, Alshaer W, Al Bawab A, Mubarak MS. Design, preparation, and characterization of effective dermal and transdermal lipid nanoparticles: A review. Cosmetics; 2021. p. 8.
65. Araujo VHS, Delello Di Filippo L, Duarte JL, Spósito L, Camargo BAF, da Silva PB, Chorilli M. Exploiting solid lipid nanoparticles and nanostructured lipid carriers for drug delivery against cutaneous fungal infections. Crit Rev Microbiol. 2020;47:79–90.
66. Patil TS, Gujarathi NA, Aher AA, Pachpande HE, Sharma C, Ojha S, Goyal SN, Agrawal YO. Recent advancements in topical Anti-Psoriatic nanostructured lipid Carrier-Based drug delivery. Int J Mol Sci 2023, 24.
67. Noor NM, Sheikh K, Somavarapu S, Taylor KMG. Preparation and characterization of dutasteride-loaded nanostructured lipid carriers coated with stearic acid-chitosan oligomer for topical delivery. Eur J Pharm Biopharm. 2017;117:372–84.
68. Rieger AM. Flow Cytometry and Cell Cycle Analysis: An Overview. In Cell-Cycle Synchronization. 2022: 47–57: Methods in Molecular Biology].

69. Iida M, Ihara S, Matsuzaki T. Hair cycle-dependent changes of alkaline phosphatase activity in the mesenchyme and epithelium in mouse vibrissal follicles. Dev Growth Differ. 2007;49:185–95.
70. Abreu CM, Reis RL, Marques AP. Dermal papilla cells and melanocytes response to physiological oxygen levels depends on their interactions. Cell Prolif. 2021;54:e13013.
71. Del Duca E, Ruano Ruiz J, Pavel AB, Sanyal RD, Song T, Gay-Mimbrera J, Zhang N, Estrada YD, Peng X, Renert-Yuval Y, et al. Frontal fibrosing alopecia shows robust T helper 1 and Janus kinase 3 skewing. Br J Dermatol. 2020;183:1083–93.
72. Wen L, Fan Z, Huang W, Miao Y, Zhang J, Liu B, Zhu D, Dai D, Zhang J, Le D, et al. Retinoic acid drives hair follicle stem cell activation via Wnt/β-catenin signalling in androgenetic alopecia. Journal of the European Academy of Dermatology and Venereology; 2024.
73. Boisvert WA, Yu M, Choi Y, Jeong GH, Zhang Y-L, Cho S, Choi C, Lee S, Lee B-H. Hair growth-promoting effect of Geranium sibiricum extract in human dermal papilla cells and C57BL/6 mice. BMC Complement Altern Med 2017, 17.
74. Andl T, Reddy ST, Gaddapara T, Millar SE. WNT signals are required for the initiation of hair follicle development. Dev Cell. 2002;2:643–53.
75. Monick MM, Carter AB, Robeff PK, Flaherty DM, Peterson MW, Hunninghake GW. Lipopolysaccharide activates Akt in human alveolar macrophages resulting in nuclear accumulation and transcriptional activity of β-Catenin. J Immunol. 2001;166:4713–20.
76. Müller-Röver S, Foitzik K, Paus R, Handjiski B, van der Veen C, Eichmüller S, McKay IA, Stenn KS. A comprehensive guide for the accurate classification of murine hair follicles in distinct hair cycle stages. J Invest Dermatology. 2001;117:3–15.
77. Xu H, Hu H, Zhao M, Shi C, Zhang X. Preparation of Luteolin loaded nanostructured lipid carrier based gel and effect on psoriasis of mice. Drug Deliv Transl Res. 2024;14:637–54.
78. Carvajal-Vidal P, González-Pizarro R, Araya C, Espina M, Halbaut L, Gómez de Aranda I, García ML, Calpena AC. Nanostructured lipid carriers loaded with Halobetasol propionate for topical treatment of inflammation: development, characterization, biopharmaceutical behavior and therapeutic efficacy of gel dosage forms. Int J Pharm 2020, 585.
79. Gilhar A, Kam Y, Assy B, Kalish RS. Alopecia areata induced in C3H/HeJ mice by interferon-gamma: evidence for loss of immune privilege. J Invest Dermatol. 2005;124:288–9.
80. Yoshida R, Tanaka K, Amagai M, Ohyama M. Involvement of the Bulge region with decreased expression of hair follicle stem cell markers in senile female cases of alopecia areata. J Eur Acad Dermatol Venereol. 2010;25:1346–50.
81. Miao L, Daozhou L, Ying C, Qibing M, Siyuan Z. A resveratrol-loaded nanostructured lipid carrier hydrogel to enhance the anti-UV irradiation and anti-oxidant efficacy. Colloids Surf B Biointerfaces. 2021;204:111786.
82. Miranda M, Pais A, Cardoso C, Vitorino C. aQbD as a platform for IVRT method development - A regulatory oriented approach. Int J Pharm. 2019;572:118695.
83. Garg NK, Tandel N, Bhadada SK, Tyagi RK. Nanostructured lipid Carrier-Mediated transdermal delivery of aceclofenac hydrogel present an effective therapeutic approach for inflammatory diseases. Front Pharmacol. 2021;12:713616.
84. Liang Y, Fan T, Bai M, Cui N, Li W, Wang J, Guan Y. Chikusetsu saponin IVa liposomes modified with a retro-enantio peptide penetrating the blood-brain barrier to suppress pyroptosis in acute ischemic stroke rats. J Nanobiotechnol. 2024;22:393.
85. Charmeau-Genevois C, Sarang S, Perea M, Eadsforth C, Austin T, Thomas P. A simplified index to quantify the irritation/corrosion potential of chemicals – Part I: skin. Regul Toxicol Pharmacol. 2021;123:104922.
86. Bai M, Cui N, Liao Y, Guo C, Li L, Yin Y, Wen A, Wang J, Ye W, Ding Y. Astrocytes and microglia-targeted Danshensu liposomes enhance the therapeutic effects on cerebral ischemia-reperfusion injury. J Control Release. 2023;364:473–89.
87. Kim JE, Lee YJ, Park HR, Lee DG, Jeong KH, Kang H: The Effect of JAK Inhibitor on the Survival, Anagen Re-Entry, and Hair Follicle Immune Privilege Restoration in Human Dermal Papilla Cells. International Journal of Molecular Sciences 2020, 21.
88. Mouna R, Broisat A, Ahmed A, Debiossat M, Boumendjel A, Ghezzi C, Kabouche Z Antiproliferative activity, cell-cycle arrest, apoptotic induction and LC-HRMS/MS analyses of extracts from two Linum species.Pharm Biol2022, 60:1491–1501.


## Publisher's note